Chapter 4

Nanoscale Switching and Degradation of Resistive Random Access Memory Studied by *In Situ* Electron Microscopy

Masashi Arita, Atsushi Tsurumaki-Fukuchi and Yasuo Takahashi

Additional information is available at the end of the chapter

http://dx.doi.org/10.5772/intechopen.69024

Abstract

The metal-filament-type resistive random access memories (ReRAMs) with copper were investigated from the point of view of dynamical microstructure evolution in the repetitive switching operations using *in situ* transmission electron microscopy (*in situ* TEM). Through a series of experiments for uncovered solid electrolyte films, stacked devices, and nanofabricated cells, formation and erasure of the copper filaments and deposits were confirmed. The behavior of the filament and deposit depended on the switching condition and history. Based on these *in situ* TEM results, the switching schematics and the degradation process were discussed.

Keywords: *in situ* transmission electron microscopy, resistive random access memory, ReRAM, conductive bridge random access memory, CBRAM, memristor, conductive filament

1. Introduction

The resistive random access memory (ReRAM) has great potential as a candidate of the next-generation nonvolatile memory because of the high-speed operation, the wide memory window, and the high-density storage per cost [1]. In addition, its capability of the multilevel or analogue memory control and its hysteretic nonlinear current-to-voltage (*I*–*V*) characteristics are suitable for the operation of the artificial neural network hardware using memristors, and this research field is very active especially in these years [2–5]. Because of these advantageous properties, vast numbers of works on ReRAMs have been reported as described in numerous review

articles [6–14]. In these years, highly integrated memory chips have been reported [15–17], and a 16 Gbits chip with 180 MB/s write and 900 MB/s read performance fabricated at the 27 nm node has already been demonstrated using the Cu-based ReRAM [18]. Commercialized or nearly commercialized ReRAM chips have also been reported [19–21]. However, there are still ambiguous issues of the switching and device degradation mechanisms, while basic principles of the ReRAM operations have been discussed using the electrochemistry of solid materials.

The ReRAM operation is performed by simply applying voltage to the device having a capacitor structure with a switching layer between the top and bottom electrodes (TE and BE) as shown in **Figure 1(a)**. The initial state of the device is typically the high-resistance state (HRS). It converts into the low-resistance state (LRS) by applying voltage (SET or "Forming" for the first SET). Subsequent voltage returns the resistance to HRS (RESET) as shown in **Figure 1(b)**. The *I–V* curves are hysteretic with the resistance ratio HRS/LRS typically 10^2 or larger (**Figure 1(c)**). The operation is called "bipolar" when the voltage polarity for SET and RESET should be reversed, while it is "unipolar" without polarity change. The ReRAM families energetically investigated have been the valence change memory (VCM) composed of a thin oxide layer between two noble electrodes, and the conductive bridging RAM (CBRAM; there are also other naming) composed of a solid electrolyte with an electrochemically active electrode (Cu or Ag) and an inactive electrode (Pt or TiN). In this report, we study some CBRAMs showing the bipolar switching as shown in **Figure 1(b)**.

The CBRAM operation has been explained based on electrical measurements and electronic and electrochemical discussions [8, 10, 14, 22]. Assuming that the TE is Cu, positive voltage to the TE generates Cu cations through oxidation of the electrode at the interface with the solid electrolyte. These cations move along the electric field and are metallized after receiving electrons at the BE interface. A Cu filament is formed there and grows toward the TE. When this filament connects two electrodes, SET switching is completed. Voltage reversal induces the opposite reaction, and the filament is ruptured (RESET). This simple model based on the results of the electrical measurements is plausible, which is an analogical model of electroplating. However, the switching details like filament evolution at SET/RESET and the behavior of the filament during device degradation are hard to be accomplished only with electrical measurements, which are important for usage of ReRAM with guaranteed reliability as the actual electronic device in the circuit.

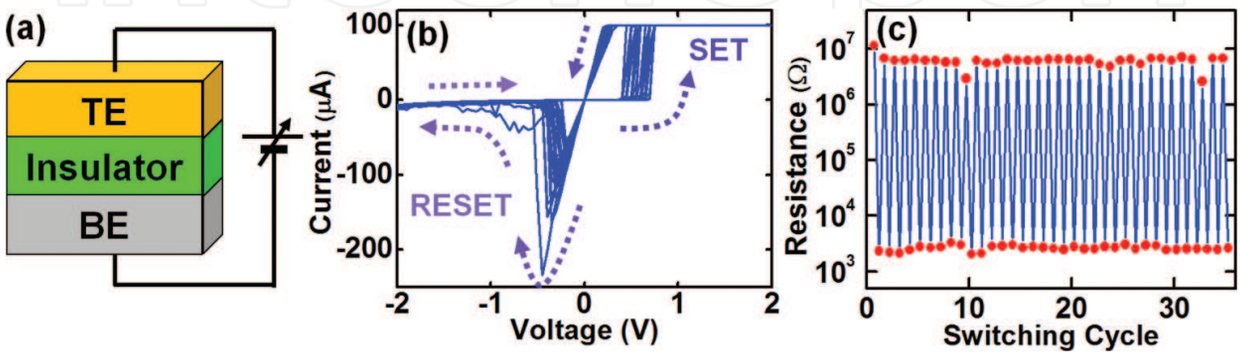

Figure 1. (a) Schematic structure of ReRAM, and typical experimental data of (b) an *I–V* switching curve and (c) a cyclic endurance graph of Cu/WO_x/TiN CBRAM cells.

http://dx.doi.org/10.5772/intechopen.69024

To overcome this problem, *in situ* transmission electron microscopy (*in situ* TEM) has been applied on a variety of ReRAMs [12, 14, 23, 24] including CBRAMs [25–29] and other families [30–37], which enable real space observations during ReRAM switching. In some examples, formation and erasure of a Cu or Ag filament were confirmed at quick switching of CBRAM [25, 27]. In another report, the filament growth scheme was categorized in terms of its dependence on the cation mobility and the reduction rate [38]. Comprehension of the filament formation has been much advanced with the sake of *in situ* TEM. On the other hand, *in situ* TEM works on RESET and the multiple operations are still rare, although they are quite important for development of reliable ReRAM devices.

For filling the lack of this knowledge, we have performed *in situ* TEM of SET/RESET and/or multiple switching cycles for an uncovered solid electrolyte, stacked CBRAMs, and nanofabricated CBRAM cells. In this contribution, we will review our work in these years [25, 29, 39–44] and discuss the role of the filament at SET/RESET, the filament growth/erasure mode influenced by the switching history, the CBRAM degradation, and the localization of the filament to achieve stable switching.

2. Experimental procedure of *in situ* TEM

A schematic diagram of the *in situ* TEM system is shown in **Figure 2(a)**. The TEM (10^{-5} Pa) was equipped with a home-made TEM piezoholder, a piezocontrol system, a current measurement unit, and a CCD camera system (30 frames/s) [45]. The Pt-Ir electrode set in the TEM holder is movable to select the location of the fixed ReRAM sample to be measured (**Figure 2(b)**). The TEM experiments were performed with the beam current density much less than the 170 fA/nm^2 (typical current density for our high-resolution TEM observations).

The *I–V* measurements were carried out using a source measure unit (SMU). The sweeping rate was typically between 0.3 and 1.6 V/s. The pulse switching operation (pulse width of

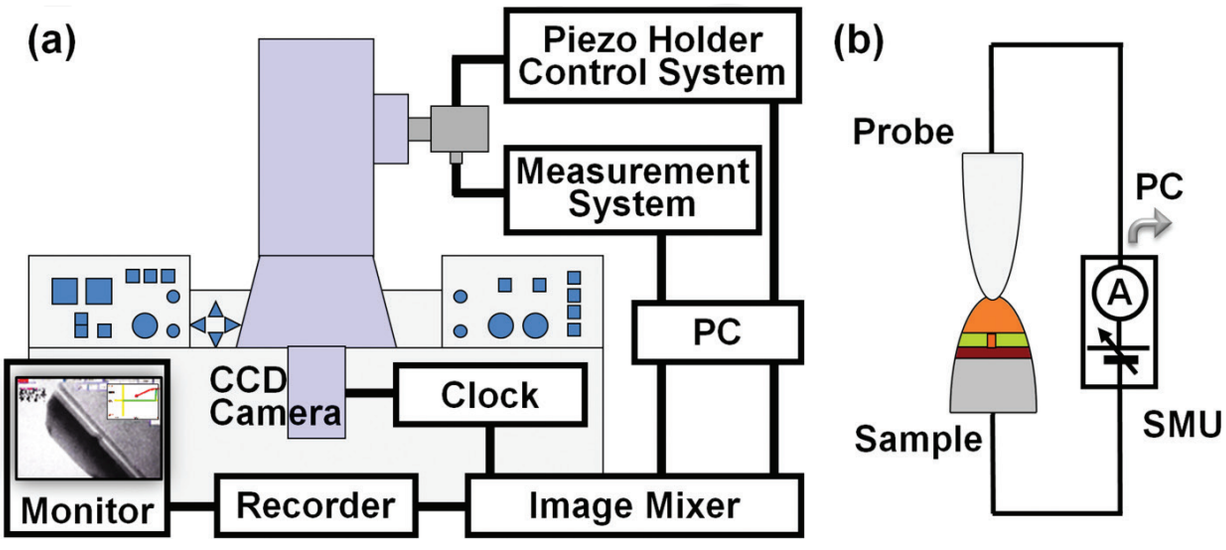

Figure 2. Schematics of (a) the *in situ* TEM system and (b) the geometry of the sample and the probe.

100–500 μs) was occasionally performed. The measurements were done with current compliance of SMU to prevent sample destruction. However, this current compliance was occasionally insufficient because of the parasitic capacitance of the system. In some cases, a MOSFET was installed in the piezoholder to control the compliance current (I_{comp}) strictly. To investigate the microstructural change, the TEM images were recorded simultaneously with the current measurements by using a charge coupled device (CCD) video camera. The video contrast was occasionally enhanced nonlinearly to enable a clear identification of the faint contrast. Frame averaging was also used to reduce the noise.

3. Filament formation and erasure in chalcogenide containing Cu

Filament formation and erasure will be demonstrated using GeS containing copper (Cu:GeS) [25, 39]. Though the switching speed and the retention property were not good enough for actual devices, this material is good for easy investigation of the filament evolution. The Cu:GeS thin film was sputter deposited at room temperature (RT) on a wedge-shaped Pt-Ir substrate that acted as the electrode. The film was 8–60 nm thick and was amorphous including Ge nanocrystals. A sharp Pt-Ir probe (the counterelectrode) contacted the Cu:GeS layer, and the *I–V* measurements were performed. The probe was grounded, and the substrate was biased. In this sample, the Cu ion source was Cu:GeS itself. The atomic composition estimated using EDX was Cu:Ge:S = 4:4:2. Though the PtIr/Cu:GeS/PtIr structure was electrochemically symmetric, it showed the asymmetric ReRAM switching (i.e., bipolar switching) because of the shape difference between the substrate and the probe.

3.1. *In situ* SET and RESET operation

The *I–V* curve is plotted in the left panel of **Figure 3**, where the current compliance was I_{comp} = 500 nA. Clear hysteretic curve was seen as investigated in other studies of solid electrolytes [6, 10, 46, 47]. TEM video images are presented in the right panel of **Figure 3** where each image corresponds to the states (a)–(i) marked in the *I–V* graph. There was no special contrast just before the voltage sweep started (**Figure 3(a)**). The current gradually increased until about 2.5 V, and a deposit-like dark contrast grew from the probe (cathode with this voltage polarity) (**Figure 3(b)–(c)**). Afterward, the current quickly reached I_{comp}. This is SET giving LRS. Correspondingly, the deposit was enlarged (**Figure 3(d)–(e)**) and contacted the substrate. In RESET with negative biasing of the substrate, there were sudden jumps at −0.5 and −2 V, which are abnormal with the usual bipolar switching. This is special for the sample without the Cu electrode (thus, amount of Cu is limited) and was neither conventional SET nor RESET [8, 10, 14, 22]. In **Figure 3(f)–(g)**, the deposit was contracted with negative voltage from the substrate (cathode) to the probe (anode). The deposit detached from the substrate in **Figure 3(h)**, and the resistance returned to HRS. This was the RESET switching. At the end of this cycle, the image reverted almost to that of the original (**Figure 3(i)**).

The deposit size and the current corresponded; therefore, this deposit is expected to act as the conductive filament. The polarity dependence may be attributed not to the electrochemical

http://dx.doi.org/10.5772/intechopen.69024

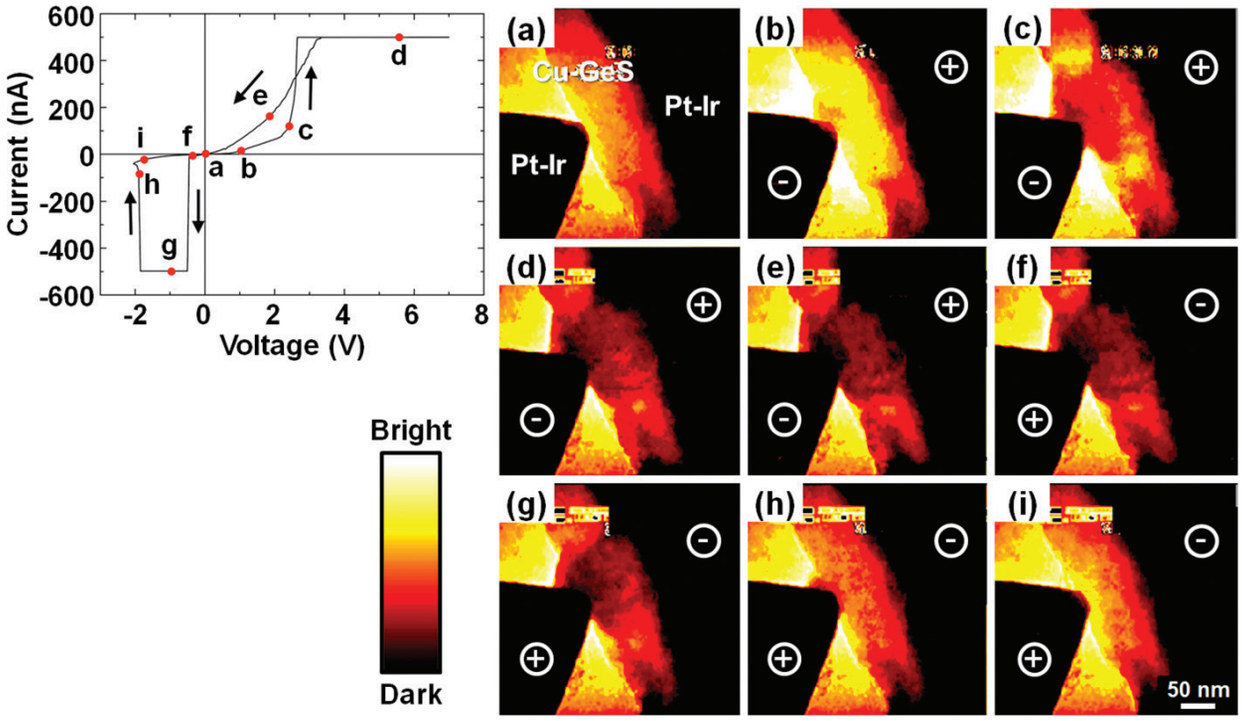

Figure 3. The switching curve (left panel) and TEM images extracted from a video (right panel) of a Cu:GeS film. The images (a)–(i) correspond to the states marked in the switching curve.

properties of the electrodes but to the asymmetry of the electric field caused by the shape difference of the electrodes. Because of the concentrated electric field, Cu ions accumulate at the probe when the substrate is positive. On the other hand, electric flux disperses toward the substrate when the polarity is reversed. Even though Cu is thought to accumulate at the substrate-film interface, its density is low for filament formation.

3.2. SAD and EDX of the conductive filament

Selected area diffractometry (SAD) and energy dispersive X-ray spectroscopy (EDX) were performed in real time during the operation (but other area than **Figure 3**). In this subsection, the results are briefly summarized. Detailed experimental data are seen in Refs. [25, 39].

The crystal structure of the filament was studied using *in situ* SAD. When a deposit was formed, sharp spots appeared in the patterns. They twinkled like stars. This indicates that nanocrystals were formed, and their orientation frequently changed during the voltage scan. The 1152 frames of the SAD video (35 s) were summed, and Debye rings were identified. The estimated *d*-values were those of Cu reflections. For the elemental analysis, the EDX of the filament was performed with voltage application (+1 V). The Cu peak was greatly enhanced relative to the initial state. The composition estimated using the thin foil approximation was Cu:Ge:S = 7:2:1, while the region containing no filaments showed 4:4:2. The filament was an agglomeration of nanocrystals with a relatively large amount of Cu; probably metallic Cu or its alloy with either Ge and/or S.

3.3. Decrease of the SET voltage and the residue of the filament

The SET voltage usually goes down after forming. This was considered to be caused by the wreckage of the filament [8, 10, 14, 22]. To understand this phenomenon, we performed three continuous SET cycles from the initial state. Because of a short retention of this sample, the deposit disappeared automatically without negative voltage. Thus, only the positive cycles were investigated. The SET voltage in the 1st, 2nd, and 3rd cycles decreased from 2.25 to 1.83 V (2nd) and 1.50 V (3rd). In this experiment, the probe position was changed as seen in **Figure 4**, where the arrows indicate the point where the probe hit in the 1st cycle. A filament appeared and disappeared at the probe in the 1st cycle (**Figure 4(a1, a2)**). Afterward, the probe was shifted as seen in **Figure 4(b1)**. When positive voltage was applied, a filament appeared elongating into the region where the 1st filament was formed. In the 3rd cycle, measurement was conducted without changing the probe position from the 2nd cycle (**Figure 4(c1)**). A filament was formed at the same place (**Figure 4 (c2)**). The region where the filament has been formed has priority in subsequent switching. Residuals of the filament should remain as extremely small metallic nanocrystals, which cannot easily be detected by SAD or conventional TEM. They are thought to act as nuclei of the filaments and to reduce the SET voltage.

3.4. Summary

The fundamental behavior of the conductive filament in Cu:GeS was demonstrated by using *in situ* TEM, *in situ* SAD, and *in situ* EDX. The switching scheme is understood as follows.

When the substrate is positively biased, Cu ions in GeS move to the cathode (probe) and a metallic deposit appears there. It consists of Cu-based nanocrystals. The deposit expanded and finally touched the anode (substrate), and the resistance state is LRS. Even in this stage, the microstructure changes with voltage application. The deposit dissolves by polarity reversal, and it shrinks from the cathode (substrate) to the anode (probe). This process gives HRS. The formation/erasure of the deposit clearly corresponded to SET/RESET. Therefore, the conductive filament must be formed in the deposit. This behavior of the filament follows the electrochemical model [8, 10, 14, 22]. With the continuation of the switching cycle, the SET voltage decreased. This is caused by the residuals (probably Cu nanocrystals) that remain even in HRS. These residues are thought to act as nuclei of the filaments.

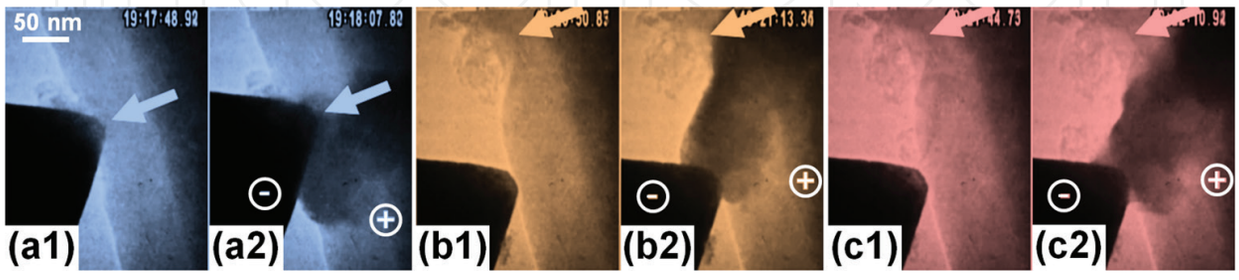

Figure 4. *In situ* TEM images of the (a) 1st, (b) 2nd, and (c) 3rd switching cycle of a Cu:GeS film. Images (a1), (b1), and (c1) are before the SET cycle, and those of (a2), (b2), and (c2) are after SET. The probe position was shifted between (a) and (b), while it was unchanged between (b) and (c). The arrow marks the potion where the probe was contacted in the 1st cycle.

4. CBRAM having the stacked structure with the Cu electrode

The special constitution of CBRAM was used in Section 3 for easy performance of experiments, such as a tip-shaped electrode and nonuse of Cu electrode. Operation was slow, and the current was much less than μA. This is satisfactory for a characterization of conductive filaments. However, to understand realistic operation, the multiple switching cycles should be achieved for multilayered CBRAMs. In Sections 5 and 6, MoO_x and WO_x sandwiched between electrochemically active Cu and inactive TiN electrodes are demonstrated. The dynamics of filament growth/shrinkage (Section 5) and device degradation (Section 6) are discussed through repetitive ReRAM operations with increase of the switching current.

The CBRAMs studied are $Pt_{(100)}/Cu_{(30)}/MoO_{x(50)}$ and $Pt_{(100)}/Cu_{(30)}/WO_{x(20)}$ on TiN/Si substrates, where the numbers denote the thicknesses in nm. Here, the TiN surface was oxidized due to the O_2 plasma treatment for cleaning. The oxide switching layers were prepared using reactive RF sputtering (Ar-20% O_2) of metal targets, while the others were by Ar RF sputtering. All depositions were done at RT without any heat treatment, and both oxides were amorphous. Typical TEM image and EDX map are shown in **Figure 5(a) and (b)**. The layer structure is clearly identified, and the overall switching area is observable. Samples for *in situ* TEM were processed using the ion-shadow method [48], where many cone-shaped small devices were formed. The device diameter was less than 500 nm as shown in **Figure 5(a)**. The current for switching was measured between the biased Pt/Cu and grounded TiN/Si. The current in the LRS was limited by the serially connected resistance of TiN/Si.

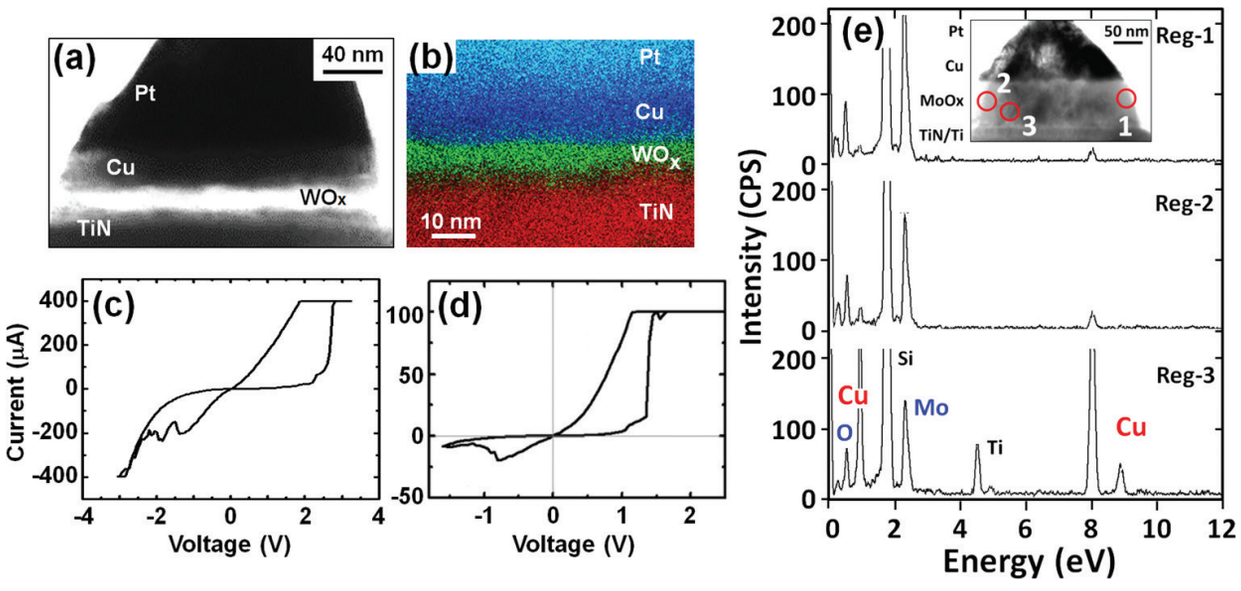

Figure 5. (a) TEM image and (b) EDX mapping of a Pt/Cu/WO_x/TiN sample where clear layer stacking was seen. The *I–V* switching curve of (c) a TEM sample (size: 350 nm) and (d) a microdevice (size: 16 μm) of Pt/Cu/MoO_x/TiN. They corresponded well to each other. (e) EDX spectra from the MoO_x layer without the filament (Reg-1 and Reg-2) and the filament (Reg-3). Enhancement of the Cu signal was clearly seen in Reg-3. Inset is the TEM image showing the analyzed areas.

Multiple switching was realized during the TEM observation. An example of the *I–V* curve measured in TEM is **Figure 5(c)**. The current gradually increased with positive voltage, and then the resistance was quickly converted to LRS. In the negative voltage region, the current exhibited jumps giving HRS. This is the typical bipolar switching as seen in **Figure 5(d)** of a conventional CBRAM device fabricated on a Si wafer using the lithography technique. The similarity of fundamental features of these graphs indicates that the vacuum environment in the TEM and electron beam irradiation had no negative effects.

Checking *in situ* TEM videos, filament-like dark contrast grew in the SET cycle and shrank/vanished in the RESET cycle. Here, this darker contrast in the oxide layer is assumed to be the Cu-based conductive filament. This assumption was confirmed by EDX for regions with/without the filament (**Figure 5(e)**). The filament was made up largely of Cu.

5. Switching operation of stacked CBRAM

In this section, the filament dynamics and its mechanism are demonstrated. The CBRAM discussed here is mainly the device having the MoO_x [29, 41, 43, 44].

5.1. Filament formation in the SET process

An example of the SET cycle is shown in **Figure 6**, where the *I–V* graph (**Figure 6(a)**) and the TEM video images (**Figure 6(b)–(g)**) are compared. The initial resistance was 40 MΩ, and thus the Cu inclusion level in MoO_x was small. For initialization, 15 positive/negative cycles were done, and the resistance decreased to 500 kΩ. Clear SET/RESET switching started after this treatment. Here, the gray contrast on the right of the image is unrelated to the switching because it showed no change of note. Increasing the voltage from state-(b), the current increased gradually. In **Figure 6(c)**, a slight change was seen near the central area. The current increased greatly at 3 V (state-(d)), and a dark contrast appeared abruptly in a wide area from the Cu electrode (**Figure 6(d)**). This gathered to be a clear contrast and connected two electrodes in **Figure 6(e)–(f)**. Its growth direction was from the anode (Cu) to the cathode (TiN), and this is opposite to the direction expected in the conventional electrochemical CBRAM

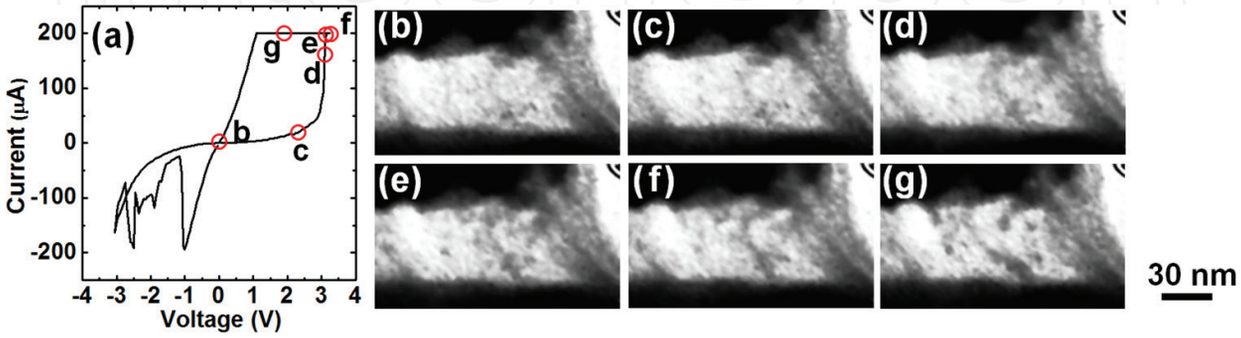

Figure 6. (a) The SET curve and (b)-(g) corresponding *in situ* TEM images of a Cu/MoO_x/TiN device with little Cu inclusion. The filament quickly grew from TE to BE.

model [8, 10, 14, 22]. This behavior has been observed in other switching materials like SiO_2 [28], ZrO_2 [27], and WO_x [42] that are thought not to dilute much Cu (or Ag). During the additional voltage application (over-SET named in this report), the filament grew further and changed its contact position with the Cu electrode toward the left (**Figure 6(g)**). Even after bridging, the filament shape continued to change. Finally, the resistance changed from 500 to 8 kΩ. The LRS retention time was longer than 5 min.

The growth direction reversed in the subsequent SET cycle (**Figure 7**). The switching started at states-(c) and (d). At this moment, there was no dramatic change in the TEM image (**Figure 7(b)–(d)**). When the current increased rapidly at state-(e), a small dark contrast appeared near the cathode (TiN). This is thought to be the nucleus of the filament. It grew, and a 35 nm thick filament bound two electrodes (**Figure 7(f)–(g)**). After the nucleus appeared, the bridging was completed within 200 ms. The resistance decreased from 750 to 8 kΩ.

To discuss the filament growing direction, five images sequentially extracted from the video (30 ms intervals) are shown in **Figure 8**. The nucleus of the filament appeared near the BE (TiN, cathode) and grew toward the TE (Cu, anode). This fits well with the electrochemical switching model [8, 10, 14, 22]. Based on the discussion in a previous report [38], the Cu ion mobility must be high in this case. This was the SET cycle after **Figure 6** (and RESET). Thus, tiny Cu residuals were expected in MoO_x at the starting of this SET. It may influence the Cu ion mobility. In addition, the Joule heat also can increase the ion mobility since large compliance current of > 10^2 A was used here.

The growth scheme from the cathode to the anode was seen also in another sample having Cu deposits near the MoO_x/TiN interface in the initial state. In this case, the initial resistance was small (700 kΩ), and Cu dissolution had happened already in the initial state. This may be caused by a temperature increase during ion milling for TEM sample preparation as seen in heat-treated Cu/SiO_2/BE [49].

Three *I–V* curves from the initial state are shown in **Figure 9(a)**. The nonhysteretic curve of the 1st cycle started to be hysteretic in the 2nd cycle. Though the resistance decreased to 400 kΩ, there was no change in the video image. In the 3rd cycle, a clear hysteresis was identified, the resistance decreased to be 30 kΩ after SET, and RESET occurred. Corresponding images (**Figure 9(b)–(d)**)

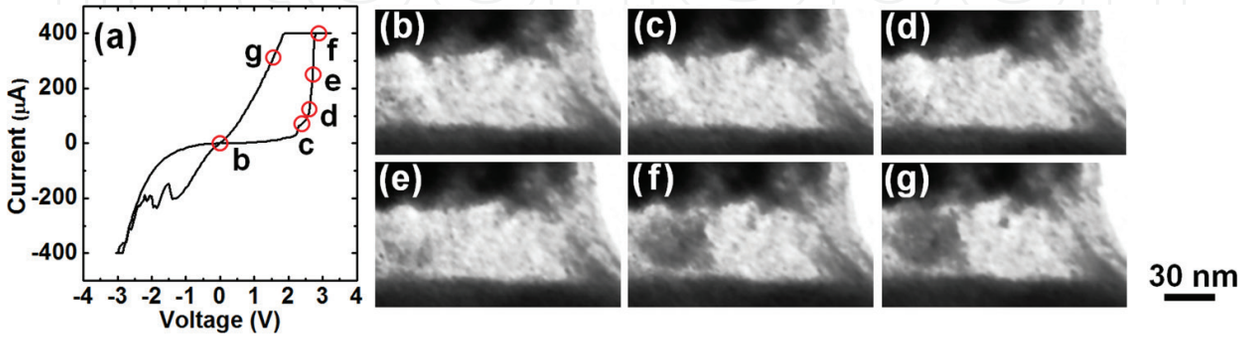

Figure 7. (a) The SET curve and (b)-(g) corresponding *in situ* TEM images of a Cu/MoO_x/TiN device when the switching layer was expected to contain a certain amount of Cu dissolution after the cycle in **Figure 6**.

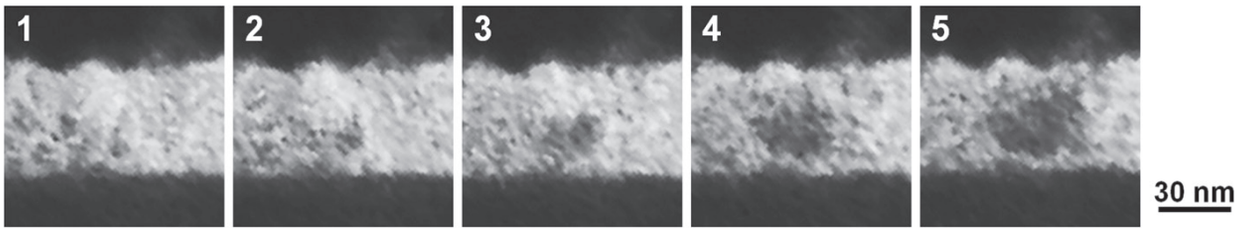

Figure 8. Details of the SET process in **Figure 7**, where the subsequent TEM video frames (images-1 to 5) were shown with the interval of 30 ms. The image-2 corresponds to **Figure 7(e)**. The Cu filament grew apparently from BE to TE.

showed a slight contrast change. The Cu deposit near ox-TiN/TiN (arrows) grew during SET (**Figure 9(c)**), and it disappeared during RESET (**Figure 9(d)**). This Cu deposit must play an important role in ReRAM.

Clear and abrupt current jumps began after the 4th and 5th cycles. The SET operation in the 6th cycle is shown in **Figure 10(a)** compared with the *in situ* TEM images (**Figure 10(b)–(g)**). A Cu deposit that grew in the 5th cycle (round contrast) was identified when the voltage sweep started (**Figure 10(b)**). There is an abrupt current jump at states-(c) and (d). However, the deposit did not show a clear change (**Figure 10(c)–(d)**). It then grew from the cathode (TiN) to the anode (Cu) with the current flow after the SET switching (over-SET) (**Figure 10(e)–(g)**). The deposit did not bridge two electrodes, although the resistance was reduced much.

Summarizing shortly, there were two SET modes with filament growths from the cathode or from the anode depending on the amount of Cu in the MoO_x layer.

5.2. Filament shrinkage and erasure in the RESET process

The RESET process after **Figure 10** is shown in **Figure 11**, where the filament had not bridged. At the states-(b) to (d) in **Figure 11(a)**, the TEM images (**Figure 11(b)–(d)**) maintained the contrast just after SET. A clear RESET switching occurred between states-(d) and (e), but the deposit shrank only slightly (**Figure 11(e)**). Continuing current flow (over-RESET named in this report),

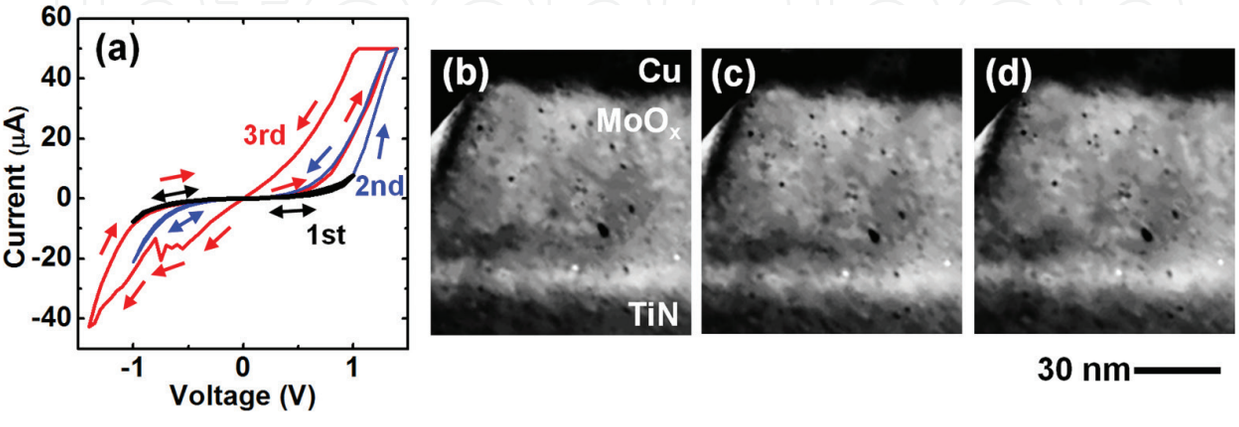

Figure 9. (a) Three *I–V* switching cycles and (b)–(d) TEM images in the 3rd cycle of a MoO_x CBRAM. The images showed appearance/disappearance of a deposit as indicated using arrows in (b) before SET, (c) after SET, and (d) after RESET.

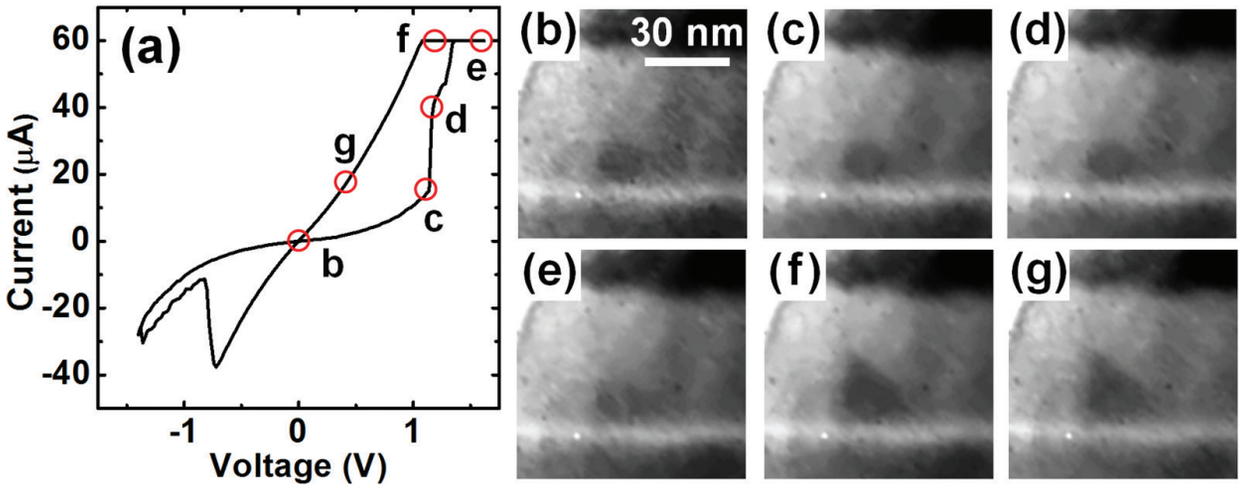

Figure 10. The 6th SET cycle performed after **Figure 9** (Cu/MoO_x/TiN). (a) *I–V* switching curve and (b)–(g) corresponding video images. Growth of the filament from BE to TE was identified.

it continued to shrink (but still not large change), toward the anode (TiN), giving roundish contrast (**Figure 11(f)** and **(g)**). The shrinkage direction fits the filament model [8, 10, 14, 22].

Figure 12 is another example of RESET with nonbridging (or weakly bridging) filament. In this example, the filament vanished due to large negative current (−600 μA, **Figure 12(a)**). The image at starting of the voltage sweep (**Figure 12(b)**) was not changed by RESET switching at state-(c) (**Figure 12(c)**). At state-(d) during over-RESET, an unexpected negative SET with large current occurred, and the filament began to shrink (**Figure 12(d)–(e)**). The filament vanished from the cathode (Cu) to the anode (TiN) (**Figure 12(f)–(g)**). Dissolution of the Cu filament was seen not only at the apex. A small precipitate near the Cu electrode (left of the images) also vanished in **Figure 12(g)**. The current spread widely and contributed to the erasure of the filament and the precipitate nearby. Although the negative SET was abnormal, we can conclude that the large negative current was required for a complete erasure of the filament.

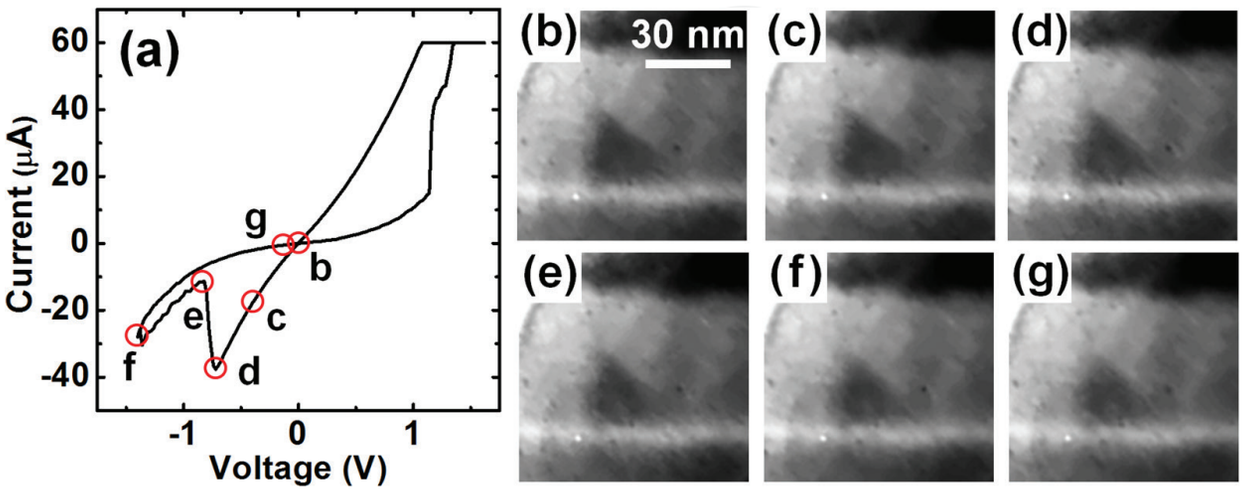

Figure 11. The 6th RESET cycle performed just after **Figure 10** (Cu/MoO_x/TiN), where the filament did not connect to the Cu TE. (a) *I–V* switching curve and (b)–(g) corresponding video images. Shrinkage of the filament from TE to BE was identified.

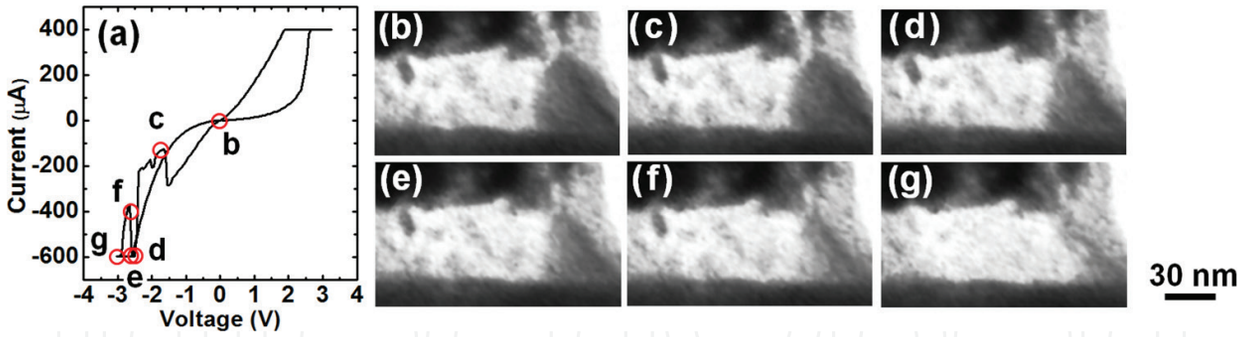

Figure 12. The RESET operation of a Cu/MoO_x/TiN where the filament did not show clear connection to the Cu TE. (a) *I–V* switching curve and (b)–(g) corresponding video images. The filament was overall erased from TE to BE during over-RESET while it did now show any change to note at the moment of RESET switching (state c).

Figure 13 is an example to show what happens for the bridging filament, which is the RESET process of **Figure 7**. With negative voltage sweep, the LRS was weakly changed by RESET before (c). The resistance further increased after another weak RESET between state-(c) and (d). However, the image of **Figure 13(d)** did not change from **Figure 13(b)–(c)**. This suggests that the RESET switching occurred locally in the filament, probably at the ends of filaments touching the electrodes [50, 51]. Through over-RESET with large negative current, the filament started to shrink (**Figure 13(e)**) and was diminished in **Figure 13(f)**. It was erased in **Figure 13(g)** although some residuals remained. A clear hysteresis was seen, and the resistance changed from 9 to 200 kΩ. The details are shown in **Figure 14** with 30 ms intervals. The filament shrank from the anode (TiN) to the cathode (Cu). This behavior did not fit with the reported filament model [8, 10, 14, 22]. The TiN surface was oxidized in this experiment, which must have higher resistance than the filament. The Joule heat concentrated in this region may assist the Cu dissolution there, and the Cu ions moved along the electric field and are adsorbed by the Cu TE.

5.3. Switching power and filament size

The current flow during RESET is an important factor to control the filament. This is true also for SET to form the conductive filament. The filament size is a key factor to affect the resistance

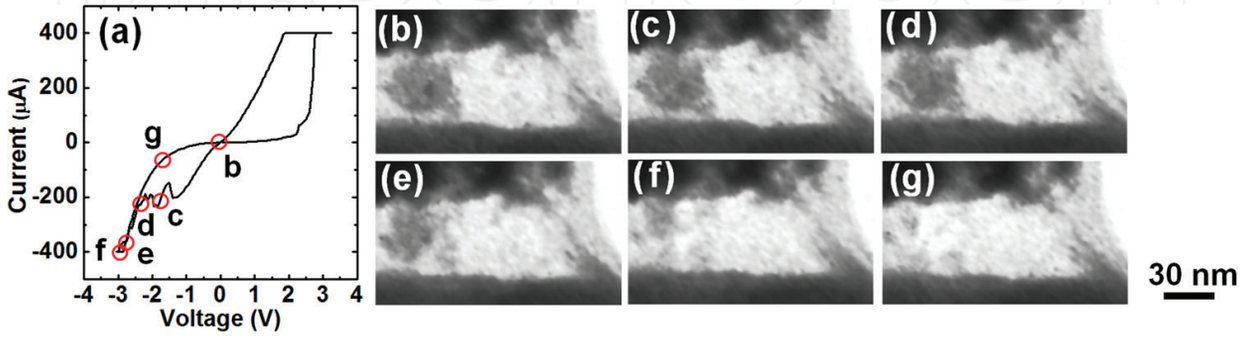

Figure 13. The RESET operation of a Cu/MoO_x/TiN when the filament bridged two electrodes. (a) *I–V* switching curve and (b)–(g) corresponding video images.

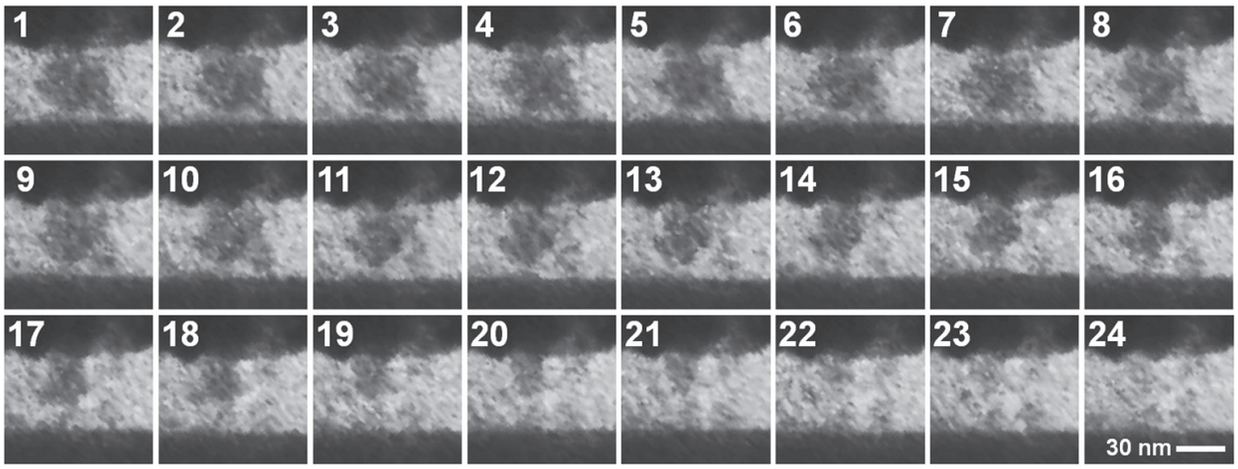

Figure 14. Details of the RESET process in **Figure 13**, where the subsequent TEM video frames (images-1 to 24) were shown with the interval of 30 ms. The Cu filament shrank apparently from BE to TE.

as well as the data retention of LRS. In this subsection, the relation between the switching power at SET and the filament size will be discussed using *in situ* TEM results.

To investigate the filament growth, five successive SET/RESET cycles were measured (**Figure 15**), where the over-SET process was gradually strengthened with increasing I_{comp}. Here, almost no over-RESET was used to prevent shrinkage of the filament. As identified in **Figure 15(a)**, the resistance gradually decreased. Corresponding TEM images acquired after SET operations are shown in **Figure 15(b)–(f)**. The filament grew step-by-step from the cathode (TiN) to the anode (Cu) with the increase of the injection power at SET. Though the resistance did not show drastic change even when the filament reached the Cu TE, it was because the resistance of TiN/Si serially connected to the switching layer limited the current.

There is a set of data with large SET current in **Figure 16**, where enough over-RESET was done to erase the filament in each cycle. During SET/RESET cycles, I_{comp} was stepwise increased to 1 mA, at which the device was destructed. **Figure 16(a)–(d)** shows the TEM images taken just after each SET. The filament in the 1st SET with I_{comp} = 200 μA was thin, and it became thick with I_{comp} (**Figure 16(e)**) as expected earlier [51, 52].

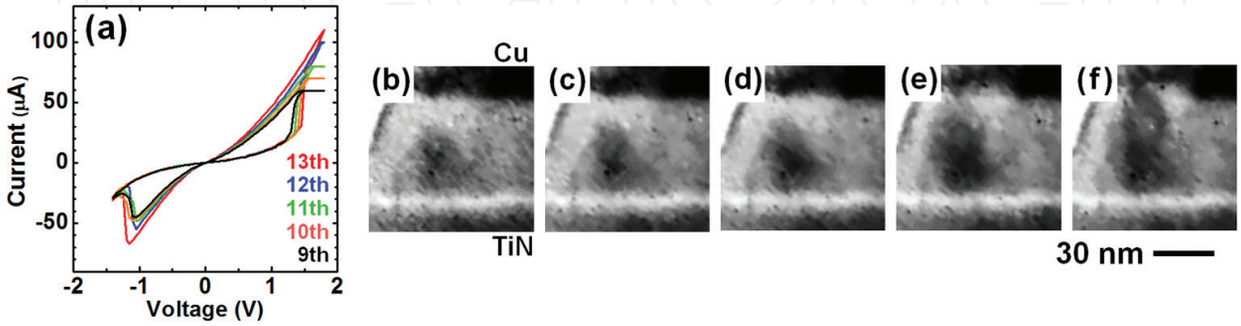

Figure 15. The 9th to 13th SET operations with increasing the compliance current (Cu/MoO_x/TiN). (a) The switching curves and the video images after SET in the (b) 9th, (c) 10th, (d) 11th, (e) 12th and (f) 13th cycles. The filament grew step by step, and the resistance decreased.

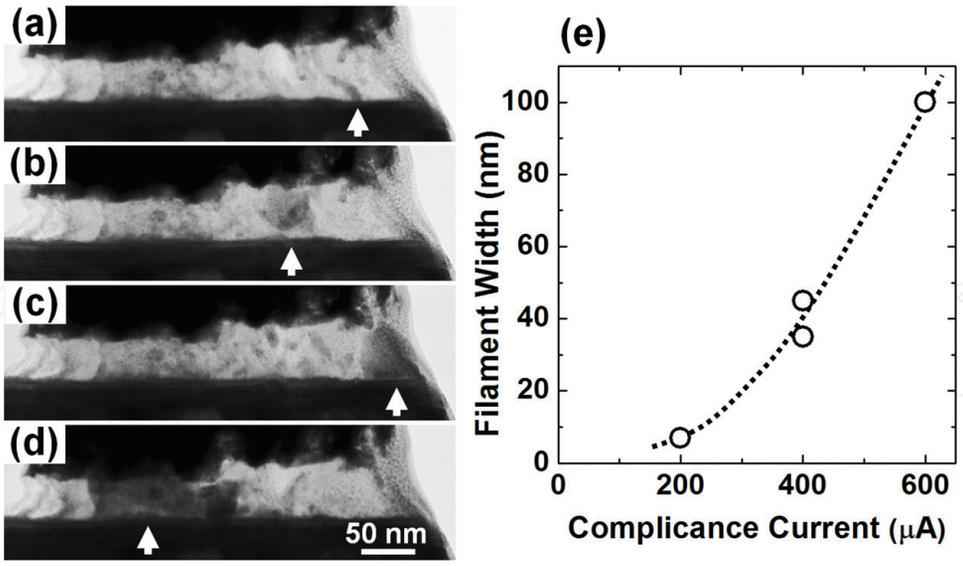

Figure 16. (a)-(d) *In situ* TEM images after SET with increasing the compliance current (a: 200, b: 400, c: 400 and d: 600 μA). After each SET, strong over-RESET was done to erase the filament. (e) Filament diameter increased with the compliance current. In addition, the filament position changed very much.

5.4. Summary of the switching schematics

Based on the results described above, SET/RESET operations are classified in **Figure 17**. There are two SET modes and two RESET modes.

When the MoO_x layer contains little Cu inclusions, a high SET voltage is required. The Cu of the anode moves quickly into MoO_x and generates deposits in a wide area, and they gather to form the filament (SET-1). When enough Cu has been dissolved in the initial state or during *I–V* cycles, the deposit appears on the TiN cathode and grows toward the Cu anode (SET-2). For enough resistance decrease, the filament connecting two electrodes is not necessarily required. The Cu^{z+} ions, oxygen vacancies and/or electrons are thought to contribute the total current. Connection of electrodes is achieved with sufficient over-SET.

There is a report on oxide CBRAMs with Ag [38]. When the Ag mobility in the oxide is low compared with the reduction rate, Ag ions are reduced to be metal before drifting for long distances, and the filament grows from the anode (Ag) to the cathode. SET-1 is categorized as this type as reported in ZrO_2 [27], SiO_2 [28] and WO_x [42]. On the other hand, when MoO_x contains sufficient Cu ions, the filament formation at the MoO_x–cathode interface can be discussed using the conventional electrochemical model [8, 10, 14, 22]. The Cu ions near the cathode can quickly reach the cathode and easily initiate the filament formation. At the same time, Cu ions are continuously generated by oxidation of the Cu electrode and supplied into MoO_x. As the result, the filament grows toward the anode (Cu). This is a plausible explanation for SET-2. A similar discussion was conducted in a previous report [53].

There are two RESET modes. The nonbridging filament tends to shrink toward the cathode (TiN). This is RESET-1. In this case, the filament acts as the anode. This transition is explained using the conventional model [8, 10, 14, 22]. The Cu filament is electrochemically dissolved in MoO_x

http://dx.doi.org/10.5772/intechopen.69024

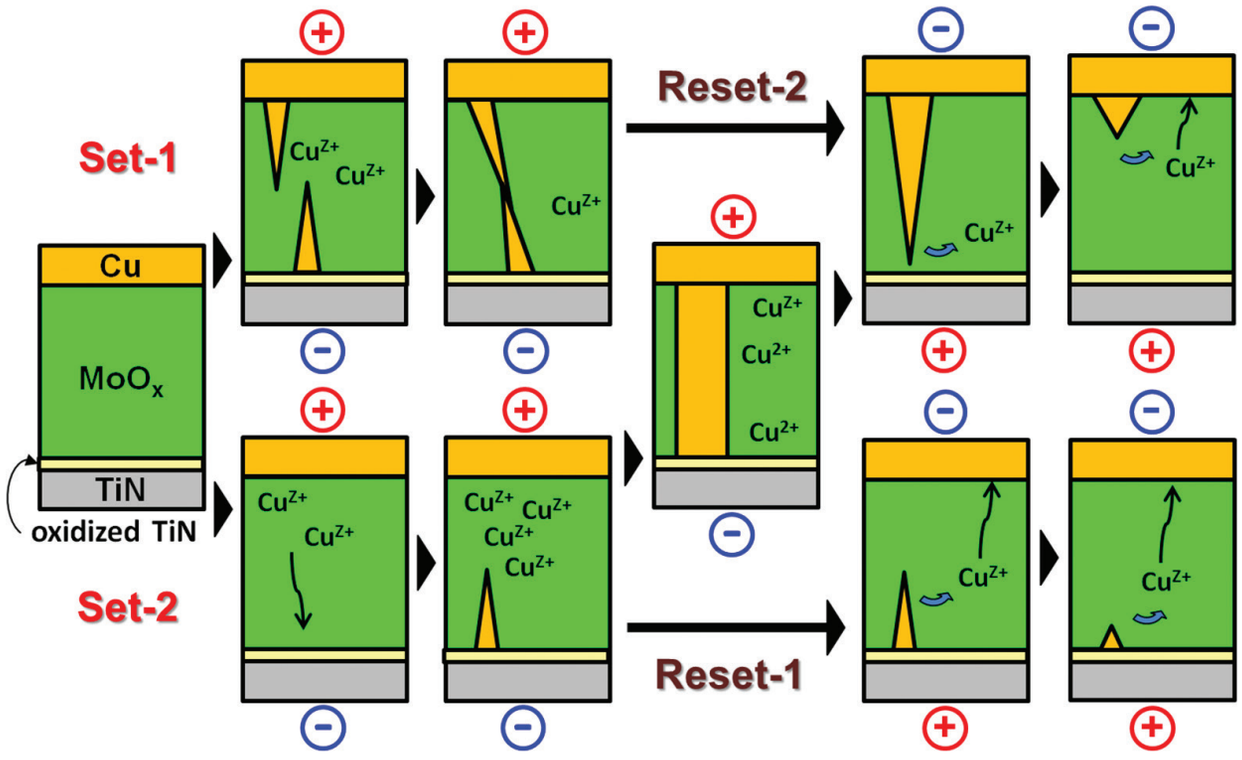

Figure 17. Switching schematics. There were two SET modes and two RESET modes.

and becomes thin overall due to widely spread current leakage. This tendency is thought to be enhanced with temperature increase during over-RESET with high current. In contrast, the filament bridging two electrodes ruptures in a region contacting with the anode (TiN); RESET-2. This is caused by the thin ox-TiN layer. The Joule heat is preferably generated near this area because of its high resistance, and Cu of the lower part of the filament is preferably dissolved in MoO_x. The dissolved ions move along the widely spread electric field. In both RESET modes, the heat generated in the filament must play an important role to the electrochemical processes.

Strictly speaking, the discussion here addresses filament formation/shrinkage during over-SET/over-RESET. Sharp resistance switching in stable *I–V* cycles can occur without such large changes. Even when the filament showed a remarkable change, this change did not occur at the moment of sharp SET/RESET switching. Stable switching occurs very locally.

5.5. Role of the interface region

As described above, large geometrical change of the filament (or deposit) was not identified at the switching moment. To check this phenomenon, the lower part of MoO_x layer was observed (**Figure 18**), where nonbridging deposit (area marked with "p" in **Figure 18(b-7)**) had been segregated at the MoO_x–ox-TiN/TiN interface. In the *I–V* measurement of **Figure 18(a)**, the switching current was less than 50 μA to prevent over-SET and over-RESET. While there was no change until **Figure 18(b2)**, the bottom edge of the Cu deposit swelled out downward into ox-TiN in state-3 after the SET switching (arrow in **Figure 18(b3)**). This faint contrast of the filament appeared to bridge the deposit and TiN as seen in **Figure 18(b4)–(b5)**. After the

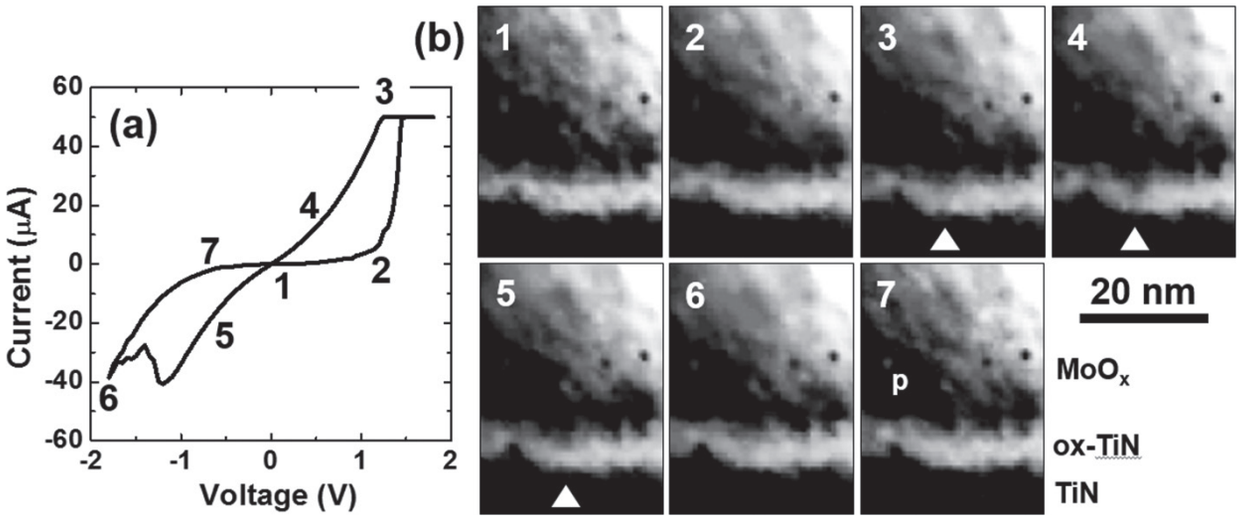

Figure 18. The SET/RESET operation showing formation/erasure of a nanofilament in thin ox-TiN at the MoO_x/TiN interface. The states 1–7 in (a) the *I–V* switching curve and (b) TEM images correspond to each other.

RESET switching around −1.5 V, this faint contrast disappeared (**Figure 18(b6)** and **(b7)**). This filament appearance/disappearance was observed at the same position also in another switching cycle. Its width was roughly 3–5 nm. Such a small filament contributes to ReRAM switching without over-SET and over-RESET. The filament in ox-TiN appeared from Cu to TiN and disappeared from TiN to Cu. The inconsistency of this phenomenon with the conventional model [8, 10, 14, 22] can be discussed with the reduction/oxidation of the Cu ions within the oxide layer [27, 28, 54] or the doping/dedoping effect [55].

This device structure is classified as a CBRAM with double switching layers like CuTe or Cu:MoO_x with GdO_x [56, 57] showing stable operation. The thick filament in the solid electrolyte may act as a narrow electrode limiting the switching region. Power control not to erase the thick filament in the solid electrolyte layer is important for stable switching repetition.

6. Device degradation

Majority of *in situ* TEM works has been done to study the switching mechanism (especially SET). They were low power switching because the slow operation makes easy observations. Considering realistic devices, studies of device reliability like data retention, endurance [58–60], and switching stability are required. For this purpose, multiple switching cycles with various currents should be performed. In this section, two device degradation tests will be demonstrated using Cu/MoO_x/TiN and Cu/WO_x/TiN. In both the examples, the operation was gradually strengthened in repetitive cycles to execute the accelerated aging tests [29, 42, 44].

6.1. Position instability of the filament after over-RESET

For an actual operation, a large resistance ratio HRS/LRS is needed. The high HRS resistance satisfies this demand. This can be achieved using over-RESET. However, the switching cycle was fatally damaged, while the stable cycle continued without it.

http://dx.doi.org/10.5772/intechopen.69024

The reason can be discussed using **Figure 16** in Section 5.3. Five SET/RESET cycles were repeated using a Cu/MoO_x/TiN CBRAM until device destruction for I_{comp} = 1 mA. The filament formed in each SET was well erased using over-RESET. A filament appeared in the 1st SET of **Figure 16(a)**, and it was erased. In the 2nd cycle with larger I_{comp}, a thicker filament appeared at the position shifted along the left (**Figure 16(b)**). Its position changed again to the right in the 3rd SET (**Figure 16(c)**). In the 4th SET, it moved to the left (**Figure 16(d)**). In the example of Section 3.3 (without over-RESET), the filament kept the position, and the tiny filament nuclei were expected as residues. On the other hand, the nuclei must be removed after the strong over-RESET in **Figure 16**. Complete erasure of the filament can give a higher resistance value in HRS, and a large memory window can be achieved. However, at the same time, it possibly induces a position change of the filament and switching instability. Power control of RESET to maintain filament residuals is thought to be important for the stable switching operation.

6.2. HRS endurance failure

Strong over-RESET induces switching instability. Therefore, the SET/RESET switching cycles were investigated on Cu/WO_x/TiN without performing over-RESET for 10 times, where the voltage was back to 0 V after the RESET switching occurred. The I_{comp} was increased stepwise from 20 to 300 μA. A large current may increase temperature and induce widely spread leakage current. Therefore, these experiments are "accelerated aging tests" under severe conditions, which is usually done before practical use of electronic devices.

Typical *I–V* curves measured in TEM are shown in **Figure 19(a)–(d)**. The characteristics of these curves are quite similar to that of a conventional device (**Figure 1(b)**, 4 μm in diameter), both of which showed the sharp bipolar switching. The difference of the switching voltage from the conventional device is caused by the small device size of the TEM sample (~210 nm). The maximum SET current (I_{comp}) and the RESET currents ($|-I_{max}|$) are summarized in **Figure 19(e)**. The current $|-I_{max}|$ tended to increase with I_{comp} as pointed out in earlier reports

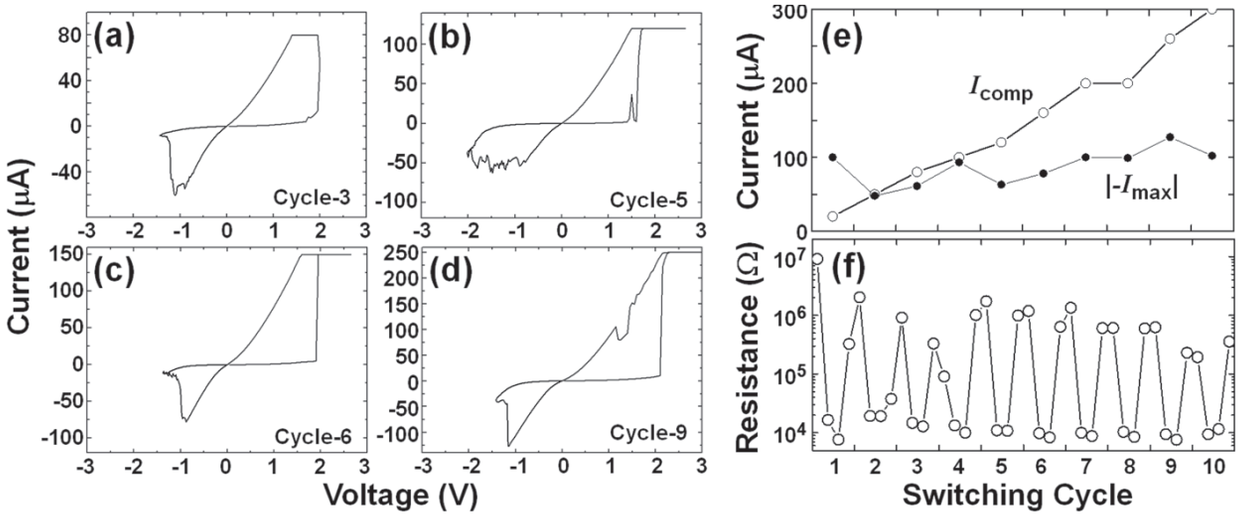

Figure 19. The SET/RESET operations of Cu/WO_x/TiN during *in situ* TEM observations. (a)–(d) Examples of *I–V* switching, (e) the relation between the compliance current I_{comp} and the maximum RESET current $|-I_{max}|$, and (f) the cyclic endurance graph where the resistances were evaluated using the *I–V* graphs both in the SET and RESET processes.

[61, 62]. The cyclic endurance is summarized in **Figure 19(f)**. The HRS/LRS resistance ratio was around 10^2. All of these properties satisfy switching fundamentals of the CBRAM devices. Thus, the *in situ* TEM results below can reflect the general ReRAM degradation property.

The resistance in the HRS gradually decreased in this graph, although the resistance ratio was still large. Here, the behavior of LRS could not be discussed because it was limited by the resistance of the serially connected substrate. Continuing the switching cycles, the device would reach HRS endurance failure as in conventional devices [58–60]. Corresponding TEM images in the initial state and after SET/RESET operations are listed in **Figure 20(a)** and **(b)–(h)**, respectively. After switching from the initial state, a filament was formed at the position marked with a triangle in **Figure 20(b)**. In the subsequent operations in **Figure 20(c)–(d)**, clear change of the filament was not identified. Afterward, small deposits grew on TiN as seen in **Figure 20(e)–(g)** with the increase of the SET current. When I_{comp} was 300 μA, a thick filament appeared at another position (**Figure 20(h)**). With the advancement of the cycles with increasing I_{comp}, the WO_x layer became thin. This indicates that current widely spread in WO_x when I_{comp} was high. The Cu moved along this current leakage and was deposited widely at the interface. Even after the filament formation, the switching layer other than the filament changes. This must be the origin of the HRS endurance failure. This failure that occurred in the operation with weak RESET was proposed to be caused by the ruptured filament tip [58, 60]. However, based on the result here, Cu tends to accumulate at the interface not only around the conductive filament.

6.3. Summary

The switching characteristics are influenced by the electric power injected into the device. High SET current enhances the filament growth and lowering of the LRS resistance as seen in **Figure 15**. Although the resistance decrease in this figure was hindered behind the substrate resistance, it will be clearly seen in **Figure 24(a)** in the next section. High HRS/LRS resistance ratio is expected in this condition. However, strong SET (or over-SET) induces unexpected Cu deposition around the filament due to Cu dissolution and movement along the widely spread current leakage. This makes the switching layer thin and the HRS endurance failure may occur. The strong RESET (or over-RESET) can recover this failure [58], which erases the filament (and deposits) and moves Cu inclusion back to the Cu electrode. However, the filament position tends to change in the next switching cycle.

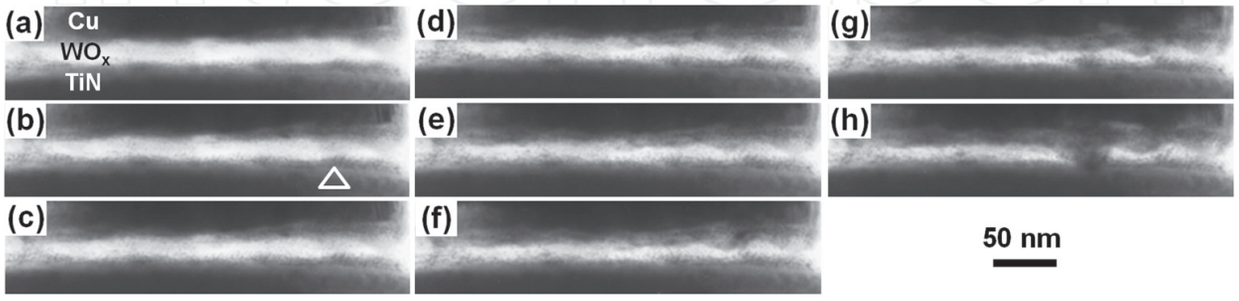

Figure 20. TEM images during device degradation of $Cu/WO_x/TiN$. The *I–V* switching cycles were performed with no over-RESET. (a) Initial, after SET/RESET of the (b) 1st (I_{comp} = 20 μA), (c) 2nd (50 μA), (d) 4th (100 μA), (e) 6th (150 μA), (f) 8th (200 μA), (g) 9th (250 μA), and (h) 10th (300 μA) cycles. The first filament was formed at the triangle in (b). The bright region corresponding to the WO_x became thin.

This may induce switching instability. The power balance of SET and RESET is important to avoid this degradation.

7. *In situ* TEM of nanofabricated CBRAM devices

Localization of the switching area may be effective to satisfy this requirement because the low power switching can be achieved without large change and easy power control of SET and RESET is expected. The nanofabricated multistacked device has a possibility to satisfy this requirement as used in the VCM [14, 63]. In this section, there is an example of *in situ* TEM of such devices [40, 41]. The evolution of the filament and Cu condensation are discussed in the nanometer range. Data retention and pulse endurance are also discussed.

Figure 21(a) is a schematic of the TEM sample. Nine devices were fabricated on a Si chip. Each CBRAM cell is composed of a Cu–Te-based solid electrolyte layer between the TE and the bottom insulator in the contact hole (30 or 70 nm). For *in situ* TEM, the device was processed by the focused ion beam technique (FIB). The current was measured between the biased TE and the grounded Si. Repetitive *I–V* cycles during *in situ* TEM are shown in **Figure 21(b)**, where 60 cycles were confirmed without degradation. The most important point is that the TEM sample reproduced the same characteristics as actual devices on memory chips.

7.1. *I–V* switching current and filament size

The *I–V* switching curves and TEM images of the 30-nm cell are tabulated in **Figure 22** where the data before and after SET and after RESET are compared for different I_{comp}. In all cases, the clear and sharp ReRAM switching was realized. In the main part of this table, the contact hole area was magnified with contrast enhancement. When I_{comp} was larger than 125 μA, contrast change due to filament formation/rupture is seen inside the insulator layer (triangle) while it could not be identified without the contrast enhancement. Other dark contrasts visible in the insulator, which did not show any change, are not related to the resistive switching and

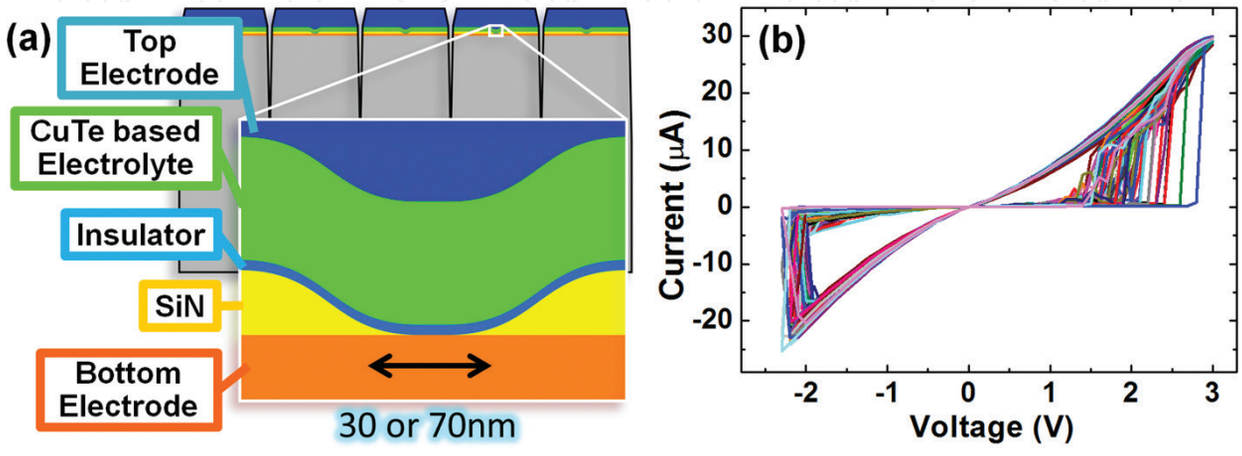

Figure 21. (a) Schematics of the nanofabricated device for *in situ* TEM, and (b) repetitive *I–V* switching (60 SET/RESET cycles) achieved in TEM.

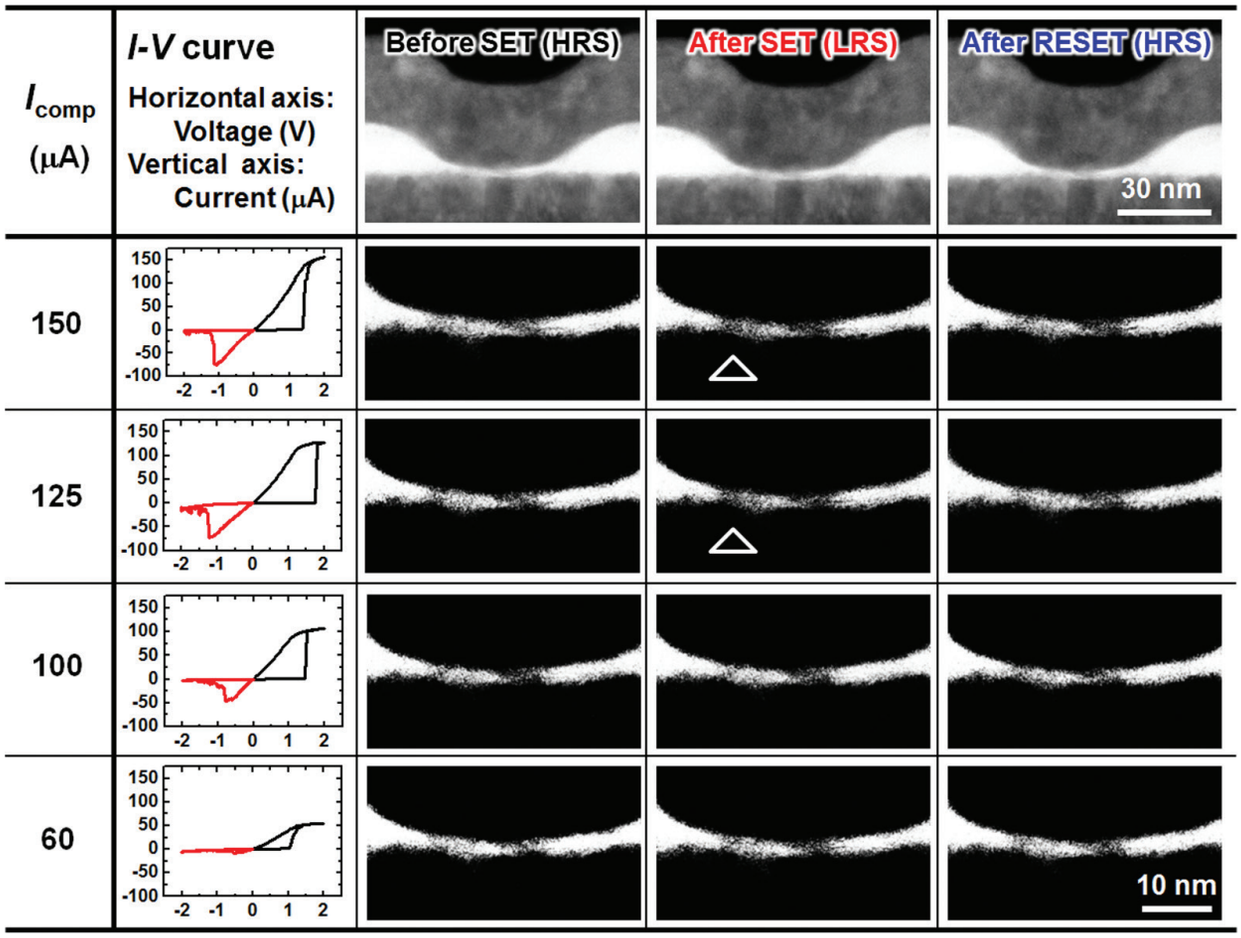

Figure 22. The *I–V* switching curve and TEM images of the 30-nm cell for various compliance current I_{comp}. The images in HRS before SET, LRS after SET, and HRS after RESET are compared. With large I_{comp}, the filament appeared and disappeared in the insulator layer (triangle).

thought to be wreckages of the solid electrolyte and/or electrodes appeared during the FIB process. The filament appeared and vanished at the same position near the edge of the contact hole. Electric field enhancement at the edge played an important role. On the other hand, no remarkable change was seen with low I_{comp}, while the SET/RESET switching was clearly seen. Very fine filaments must be formed in these cases.

7.2. Accumulation of Cu

To perform the elementary analyses, the EDX mapping was done. The results are shown in **Figure 23**, where the data in the initial state and after the SET with I_{comp} = 60 μA of the 70-nm cell, and after SET with I_{comp} = 450 μA of the 30-nm cell are compared.

In the initial state, both Cu and Te maps showed uniform distribution in the solid electrolyte layer. Little change in the distribution was observed for either Cu or Te after SET (60 μA) where a clear filament could not be seen in the TEM image. However, gathering of Cu was observed at the left end of the contact hole at SET with I_{comp} = 450 μA. In addition, the Cu moved and accumulated in the insulator layer. This was not seen in the Te map, where the insulator layer with a white contrast is still visible. This suggests that only Cu ions moved into

http://dx.doi.org/10.5772/intechopen.69024

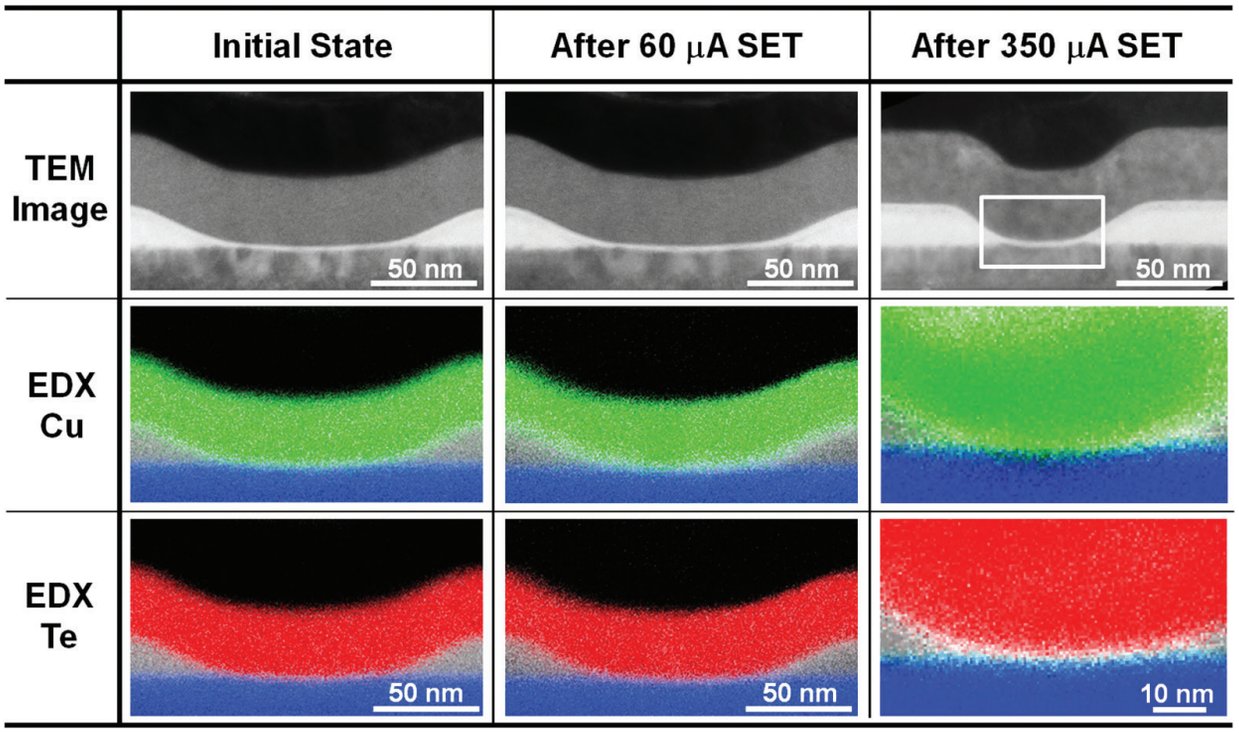

Figure 23. TEM images and EDX maps (Cu and Te) of three devices. Initial state and two SET processes with different I_{comp} are compared. In the right column, the square region in the TEM image was analyzed by EDX. When current was large, Cu movement into the insulator layer was identified. Note the magnification of the EDX maps are not constant..

the insulator by the electric field at SET. This is consistent with the filament formation shown in **Figure 22** and the model predicted in a previous report of the similar double-layer CBRAM device [56]. These results prove that resistive switching here was a result of a formation process of the Cu filament as discussed in the previous section.

7.3. Data retention and pulse endurance

Resistance variation after SET for various I_{comp} is shown in **Figure 24(a)**. The LRS formed with $I_{comp} \geq 40$ μA showed a good retention (more than 3×10^6 s = 3 months). Even with a small SET current generating very thin filament that was hard to be observed, a good retention could be achieved when the filament was localized in the thin insulator. The HRS retention capability was also confirmed to be more than 3 months because it is more stable than LRS. An additional issue can be discussed using **Figure 24(a)**. The resistance just after SET decreased with I_{comp}. This was caused by the thickened filament with large I_{comp} as shown in **Figure 22**.

Repeatable pulse-voltage operation is another issue to be investigated. A pulse endurance graph during *in situ* TEM is shown in **Figure 24(b)**. About 10^5 pulse switching cycles were achieved inside the TEM without any damage. These results clearly show that CBRAMs worked normally even during TEM experiments.

7.4. Summary

Considering the practical application, the switching operations of nanofabricated Cu-Te cells were explained in this section. Adopting the structure with double switching layers, the Cu

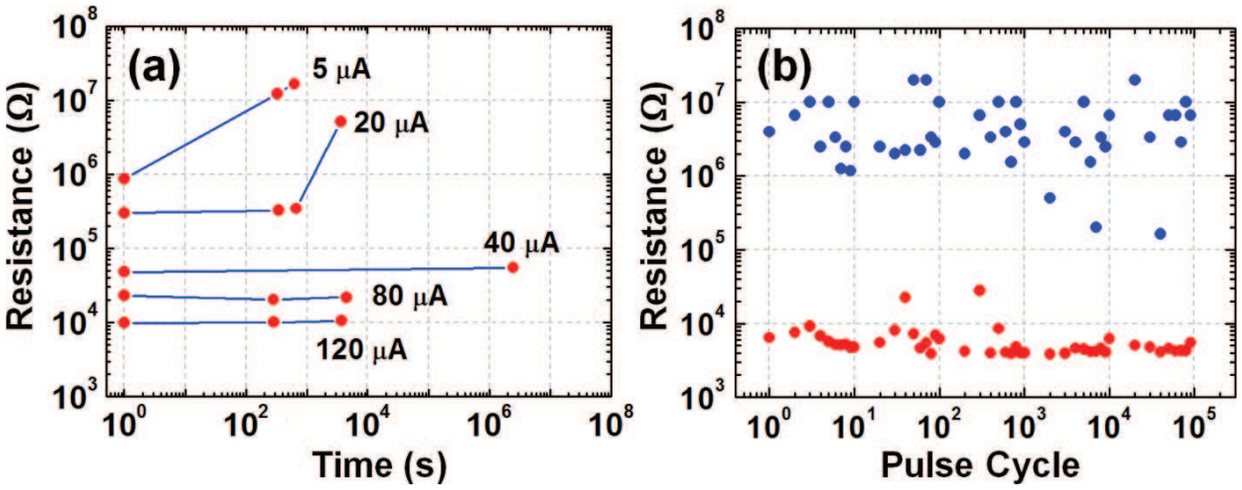

Figure 24. Reliability test performed during *in situ* TEM. (a) The LRS retention graph after SET with various compliance currents, where the read voltage was +0.2 V. (b) The pulse endurance graph. The pulse voltage and width were +3.0 V and 500 μs (for SET) or −1.5 V and 100 μs (for RESET).

nanofilament can be localized in the thin insulator, and a sharp switching can be achieved with a low current. The accumulation of Cu in the Cu-Te layer forms a thicker filament than the one in the insulator, and it acts as a miniaturized Cu electrode that limits the switching area. Increasing the switching current, the filament becomes thick for easy TEM observations, and the retention property improves. Selecting optimum operation condition, the 10^5 pulse switching and long retention over 3 months are possible during *in situ* TEM. The double-layer CBRAM can limit the switching area with short amount of Cu movement. This must be the key factor to realize stable and sharp switching properties.

8. Concluding remarks

In this contribution, we reviewed our recent *in situ* TEM works of various CBRAMs; uncovered Cu:GeS contacted with a needle-shaped electrode, stacked Cu/MoO_x/TiN or Cu/WO_x/TiN, and the nanofabricated Cu–Te-based ReRAM cell.

In all cases, the Cu conductive filament appeared in the SET process and shrank/vanished in the RESET process. There were two SET modes and two RESET modes. The growth/erasure direction of the filament depended on the switching history especially the amount of Cu dissolved in the switching layer. However, in the *I–V* switching cycles, the filament did not necessarily show remarkable change in geometry at the SET/RESET switching moment. The local area near the electrode is thought to contribute this switching. *In situ* TEM in nanometer or subnanometer scale is necessary for a detailed understanding of the filament evolution.

The Cu filament grew/shrank much during over-SET/over-RESET. For such a large change, the operation current (and accompanied temperature increase) seems to play an important role. With a current increase at SET, the filament became thick and the LRS resistance decreased. However, when strong RESET was not operated, influence of widely spread leakage current

http://dx.doi.org/10.5772/intechopen.69024

became conspicuous, and unexpected Cu deposits were formed widely at the interface. This reduced the effective thickness of the switching layer and lead to the HRS endurance failure. While strong RESET may prevent this degradation, the filament position changed under this condition, and the switching became unstable. The switching powers at SET and RESET should be balanced for clear and stable ReRAM switching.

This was realized by adopting miniaturized CBRAM cells with double switching layers. The thin filament in nm range was localized in a thin insulator layer, while thicker Cu condensation occurred in the solid electrolyte, which could act as a protrusion of the electrode. Sharp and stable switching was performed with low current, and less degree of Cu movement was expected. This sharp switching property is applicable for conventional binary memories. On the other hand, the sharp switching is not ideal for application of the artificial neural networks that require multilevel or analogue control of the resistance. Further device designing is needed to perform stable operation for this type of devices.

The operation failure is the critical issue to ensure the practical application of ReRAMs. It is indispensable to clarify main origins of the malfunction and to guarantee device reliability. We demonstrated many *in situ* TEM functions that are available for reliability tests: *I–V* characteristics, pulse switching, endurance, and data retention. While the time resolution is limited by the video frame rate (30 ms/frame in usual cases), other functions like TEM or scanning TEM (STEM) imaging as well as the elementary or chemical analyses using EDX or electron energy loss spectroscopy (EELS) are possible. *In situ* TEM is applicable to characterize nanometer-scale ReRAM cells expected for gigabit scale integration.

Acknowledgements

We acknowledge the financial support from the Japan Society for the Promotion of Science (JSPS, KAKENHI, 15H01706, 16H0433906, and 16K18073). This work was partly performed under the Nanotechnology Platform Program (Hokkaido Univ. and Kyushu Univ.) organized by the Ministry of Education, Culture, Sports, Science, and Technology (MEXT), Japan. Part of this work was carried out under the collaboration with the Semiconductor Technology Academic Research Center (STARC) as well as Sony Corp. We are grateful to Messer Kouichi Hamada and Yuji Mori for development of the experimental setup, especially piezo-TEM holders. Finally, we would like to emphasize that the works reviewed here could not be accomplished without the collaboration with our laboratory members.

Author details

Masashi Arita*, Atsushi Tsurumaki-Fukuchi and Yasuo Takahashi

*Address all correspondence to: arita@nano.ist.hokudai.ac.jp

Laboratory of Nanomaterial Engineering, Graduate School of Information Science and Technology, Hokkaido University, Sapporo, Japan

References

[1] Sacchetto D, Gaillardon PE, Zervas M, Carrara S, De Micheli G, Leblebici Y. Applications of multi-terminal memristive devices: A review. IEEE Circuits and Systems Magazine. 2013;**13**(2):23-41. DOI: 10.1109/MCAS.2013.2256258

[2] Seo K, Kim I, Jung S, Jo M, Park S, Park J, et al. Analog memory and spike-timing-dependent plasticity characteristics of a nanoscale titanium oxide bilayer resistive switching device. Nanotechnology. 2011;**22**(25):254023. DOI: 10.1088/0957-4484/22/25/254023

[3] Nayak A, Ohno T, Tsuruoka T, Terabe T, Hasegawa T, Gimzewski JK, Aono M. Controlling the synaptic plasticity of a Cu_2S gap-type atomic switch. Advanced Functional Materials. 2012;**22**(17):3606-3613. DOI: 10.1002/adfm.201200640

[4] Prezioso M, Merrikh-Bayat F, Hoskins BD, Adam GC, Likharev KK, Strukov DB. Training and operation of an integrated neuromorphic network based on metal-oxide memristors. Nature. 2015;**521**(7550):61-64. DOI: 10.1038/nature14441

[5] DeSalvo B, Vianello E, Garbin D, Bichler O, Perniola L. From memory in our brain to emerging resistive memories in neuromorphic systems. In: 2015 IEEE 7th International Memory Workshop; May 17-20, 2015; Monterey, CA, USA. Piscataway, NJ, USA: IEEE; 2015. pp. 9-12. DOI: 10.1109/IMW.2015.7150286

[6] Waser R, Aono M. Nanoionics-based resistive switching memories. Nature Materials. 2007;**6**(11):833-840. DOI: 10.1038/nmat2023

[7] Sawa A. Resistive switching in transition metal oxides. Materials Today. 2008;**11**(8):28-36. DOI: 10.1016/S1369-7021(08)70119-6

[8] Waser R, Dittmann R, Staikov G, Szot K. Redox-based resistive switching memories – Nanoionic mechanisms, prospects, and challenges. Advanced Materials. 2009;**21**(25-26): 2632-2663. DOI: 10.1002/adma.200900375

[9] Akinaga H, Shima H. Resistive random access memory (ReRAM) based on metal oxides. Proceedings of the IEEE. 2010;**98**(12):2237-2251. DOI: 10.1109/JPROC.2010.2070830

[10] Chen A. Ionic memory technology. In: Kharton VV, editor. Solid State Electrochemistry II: Electrodes, Interfaces and Ceramic. 1st ed. Weinheim, Germany: Wiley-VCH; 2011. pp. 1-30. DOI: 10.1002/9783527635566.ch1

[11] Kim KM, Jeong DS, Hwang CS. Nanofilamentary resistive switching in binary oxide system; a review on the present status and outlook. Nanotechnology. 2011;**22**(25):254002. DOI: 10.1088/0957-4484/22/25/254002

[12] Yang Y, Lu W. Nanoscale resistive switching devices: Mechanisms and modeling. Nanoscale. 2013;**5**:10076-10092. DOI: 10.1039/c3nr03472k

[13] Mickel PR, Lohn AJ, Marinella MJ. Memristive switching: Physical mechanisms and applications. Modern Physics Letters B. 2014;**28**(10):1430003

[14] Pan F, Gao S, Chen C, Song C, Zeng F. Recent progress in resistive random access memories: Materials, switching mechanisms, and performance. Materials Science and Engineering R. 2014;**83**:1-59. DOI: 10.1142/S0217984914300038

[15] Liu TY, Yan TH, Scheuerlein R, Chen Y, Lee JKY, Balakrishnan G, et al. A 130.7mm^2 2-layer 32Gb ReRAM memory device in 24nm technology. In: Fujino LC, editor. 2013 IEEE Solid-State Circuits Conference (ISSCC): Digest of Technical Papers; Feb. 17-21, 2013; San Francisco, CA, USA. Piscataway, NJ, USA: IEEE; 2013. pp. 210-212. DOI: 10.1109/ISSCC.2013.6487703

[16] Fackenthal R, Kitagawa M, Otsuka W, Prall K, Mills D, Tsutsui K, et al. A 16Gb ReRAM with 200MB/s write and 1GB/s read in 27nm technology. In: Fujino LC, editor. 2014 IEEE International Solid-State Circuits Conference (ISSCC): Digest of Technical Papers; Feb. 9-13, 2014; San Francisco, CA, USA. Piscataway, NJ, USA: IEEE; 2014. pp. 338-340. DOI: 10.1109/ISSCC.2014.6757460

[17] Business Korea. Samsung Successfully Develops 3D Cross Point Memory [Internet]. Feb. 12, 2016. Available from: http://www.businesskorea.co.kr/english/news/ict/13818-chasing-intel-samsung-successfully-develops-3d-cross-point-memory [Accessed: Feb. 24, 2017]

[18] Sills S, Yasuda S, Calderoni A, Cardon C, Strand J, Aratani K, Ramaswamy N. Challenges for high-density 16Gb ReRAM with 27nm technology. In: 2015 Symposium on VLSI Technology: Digest of Technical Papers; 16-18 June 2015; Kyoto, Japan. Piscataway, NJ, USA: IEEE; 2015. pp. T106-T107. DOI: 10.1109/VLSIT.2015.7223639

[19] Nikkei Asian Review. Panasonic, UMC Join to Make Advanced Power-saving Memory [Internet]. Feb. 1, 2017. Available from: http://asia.nikkei.com/Tech-Science/Tech/Panasonic-UMC-join-to-make-advanced-power-saving-memory [Accessed: 23-02-2017]

[20] Hihara H, Tamagawa N, Imamura T, Sugaya H, Sugibayashi T, Miyamura M, et al. Programmable SpaceWire interface with atom switch. In: Parkes S, Carrie C, editors. 2016 International SpaceWire Conference Proceedings; Oct. 24-28, 2016; Yokohama, Japan. Piscataway, NJ, USA: IEEE; 2016. DOI: 10.1109/SpaceWire.2016.7771606

[21] Fujitsu Semiconductor. Fujitsu Semiconductor Launches World''s Largest Density 4 Mbit ReRAM Product for Mass Production [Internet]. Oct. 26, 2016. Available from: http://www.fujitsu.com/jp/group/fsl/en/resources/news/press-releases/2016/1026.html [Accessed: 23-02-2017]

[22] Goux L, Valov I. Electrochemical processes and device improvement in conductive bridge RAM cells. Physica Status Solidi A. 2016;**213**(2):274-288. DOI: 10.1002/pssa. 201532813

[23] Strobel J, Neelisetty KK, Chakravadhanula VSK, Kienle L. Transmission electron microscopy on memristive devices: An overview. Applied Microscopy. 2016;**46**(4):206-216. DOI: 10.9729/AM.2016.46.4.206

[24] Yang Y, Takahashi Y, Tsurumaki-Fukuchi A, Arita M, Moors M, Buckwell M, et al. Probing electrochemistry at the nanoscale: In situ TEM and STM characterizations of conducting filaments in memristive devices. Journal of Electroceramics (online Feb. 11, 2017) 2017;DOI: 10.1007/s10832-017-0069-y

[25] Fujii T, Arita M, Takahashi Y, Fujiwara I. In situ transmission electron microscopy analysis of conductive filament during solid electrolyte resistance switching. Applied Physics Letters. 2011;**98**(21):212104. DOI: 10.1063/1.3593494

[26] Choi SJ, Park GS, Kim K-H, Cho S, Yang WY, et al. In situ observation of voltage-induced multilevel resistive switching in solid electrolyte memory. Advanced Materials. 2011;**23**(29):3272-3277. DOI: 10.1002/adma.201100507

[27] Liu Q, Sun J, Lv H, Long S, Yin K, Wan N, et al. Real-time observation on dynamic growth/dissolution of conductive filaments in oxide-electrolyte-based ReRAM. Advanced Materials. 2012;**24**(14):1844-1849. DOI: 10.1002/adma.201104104

[28] Yang Y, Gao P, Gaba S, Chang T, Pan X, Lu W. Observation of conducting filament growth in nanoscale resistive memories. Nature Communications. 2012;**4**:732. DOI: 10.1038/ncomms1737

[29] Kudo M, Arita M, Ohno Y, Takahashi Y. Filament formation and erasure in molybdenum oxide during resistive switching cycles. Applied Physics Letters. 2014;**105**(17):173504. DOI: 10.1063/1.4898773

[30] Jooss Ch, Hoffmann J, Fladerer J, Ehrhardt M, Beetz T, Wu L, Zhu Y. Electric pulse induced resistance change effect in manganites due to polaron localization at the metal-oxide interfacial region. Physical Review B. 2008;**77**(13):132409. DOI: 10.1103/PhysRevB.77.132409

[31] Fujii T, Kaji H, Kondo H, Hamada K, Arita M, Takahashi Y. I-V hysteresis of $Pr_{0.7}Ca_{0.3}MnO_3$ during TEM observation. IOP Conference Series: Materials Science and Engineering. 2010;**8**:012033. DOI: 10.1088/1757-899X/8/1/012033

[32] Yang Y, Lu W, Yao Y, Sun J, Gu C, Gu L, et al. In situ TEM observation of resistance switching in titanate based device. Scientific Reports. 2014;**4**:3890. DOI: 10.1038/srep03890

[33] Kwon DH, Kim KM, Jang JH, Jeon JM, Lee MH, Kim GH, et al. Atomic structure of conducting nanofilaments in TiO_2 resistive switching memory. Nature Nanotechnology. 2010;**5**:148-153. DOI: 10.1038/NNANO.2009.456

[34] Fujii T, Arita M, Hamada K, Kondo H, Kaji H, Takahashi Y, et al. I-V measurement of NiO nanoregion during observation by transmission electron microscopy. Journal of Applied Physics. 2011;**109**(5):053702. DOI: 10.1063/1.3553868

[35] Chen JY, Hsin CL, Huang CW, Chiu CH, Huang YT, Lin SJ, et al. Dynamic evolution of conducting nanofilament in resistive switching memories. Nano Letters. 2013;**13**(8):3671-3677. DOI: 10.1021/nl4015638

[36] Park GS, Kim YB, Park SY, Li XS, Heo S, Lee MJ, et al. In situ observation of filamentary conducting channels in an asymmetric Ta_2O_{5-x}/TaO_{2-x} bilayer structure. Nature Communications. 2013;**4**:2382. DOI: 10.1038/ncomms3382

[37] Fujii T, Arita M, Hamada K, Takahashi Y, Sakaguchi N. In-situ transmission electron microscopy of conductive filaments in NiO resistance random access memory and its analysis. Journal of Applied Physics. 2013;**113**(8):083701. DOI: 10.1063/1.4792732

[38] Yang Y, Gao P, Li L, Pan X, Tappertzhofen S, Choi SH, et al. Electrochemical dynamics of nanoscale metallic inclusions in dielectrics. Nature Communications. 2014;**5**:4232. DOI: 10.1038/ncomms5232

[39] Fujii T, Arita M, Takahashi Y, Fujiwara I. Analysis of resistance switching and conductive filaments inside Cu-Ge-S using in situ transmission electron microscopy. Journal of Materials Research. 2012;**27**(6):886-896. DOI: 10.1557/jmr.2011.437

[40] Kudo M, Arita M, Takahashi Y, Ohba K, Shimuta M, Fujiwara I. Visualization of conductive filament during write and erase cycles on nanometer-scale ReRAM achieved by in-situ TEM. In: 2015 IEEE 7th International Memory Workshop; May 17-20, 2015; Monterey, CA, USA. Piscataway, NJ, USA: IEEE; 2015. pp. 85-88. DOI: 10.1109/IMW.2015.7150312

[41] Takahashi Y, Kudo M, Arita M. Visualization of conductive filament of ReRAM during resistive switching by in-situ TEM. ECS Transactions. 2015;**69**(10):299-309. DOI: 10.1149/06910.0299ecst

[42] Arita M, Takahashi A, Ohno Y, Nakane A, Tsurumaki-Fukuchi A, Takahashi Y. Switching operation and degradation of resistive random access memory composed of tungsten oxide and copper investigated using in-situ TEM. Scientific Reports. 2015;**5**:17103. DOI: 10.1038/srep17103

[43] Arita M, Ohno Y, Takahashi Y. Switching of Cu/MoO_x/TiN CBRAM at MoO_x/TiN interface. Physica Status Solidi A. 2016;**213**(2):306-310. DOI: 10.1002/pssa.201532414

[44] Arita M, Ohno Y, Murakami Y, Takamizawa K, Tsurumaki-Fukuchi A, Takahashi Y. Microstructural transitions in resistive random access memory composed of molybdenum oxide with copper during switching cycles. Nanoscale. 2016;**8**:14754-14766. DOI: 10.1039/c6nr02602h

[45] Arita M, Hamada K, Takahashi Y, Sueoka K, Shibayama T. In situ transmission electron microscopy for electronics. In: Khan M, editor. The Transmission Electron Microscope - Theory and Applications. Rijeka, Croatia: InTech; 2015. pp. 35-68. DOI: 10.5772/60651

[46] Kozicki MN, Park M, Mitkova M. Nanoscale memory elements based on solid-state electrolytes. IEEE Transactions on Nanotechnology. 2005;**4**(3):331-338. DOI: 10.1109/TNANO.2005.846936

[47] Sakamoto T, Lister K, Banno N, Hasegawa T, Terabe K, Aono M. Electronic transport in Ta_2O_5 resistive switch. Applied Physics Letters. 2007;**91**(9):092110. DOI: 10.1063/1. 2777170

[48] Kudo M, Arita M, Ohno Y, Fujii T, Hamada K, Takahashi Y. Preparation of resistance random access memory samples for in situ transmission electron microscopy experiments. Thin Solid Films. 2013;**533**:48-53. DOI: 10.1016/j.tsf.2012.10.102

[49] Thermadam SP, Bhagat SK, Alford TL, Sakaguchi Y, Kozicki MN, Mitkova M. Influence of Cu diffusion conditions on the switching of Cu–SiO_2-based resistive memory devices. Thin Solid Films. 2010;**518**:3293-3298. DOI: 10.1016/j.tsf.2009.09.021

[50] Tsuruoka T, Terabe K, Hasegawa T, Aono M. Forming and switching mechanisms of a cation-migration-based oxide resistive memory. Nanotechnology. 2010;**21**(42):425205. DOI: 10.1088/0957-4484/21/42/425205

[51] Bernard Y, Renard VT, Gonon P, Jousseaume V. Back-end-of-line compatible conductive bridging RAM based on Cu and SiO_2. Microelectronic Engineering. 2011;**88**(5):814-816. DOI: 10.1016/j.mee.2010.06.041

[52] Russo U, Kamalanathan D, Ielmini D, Lacaita AL, Kozicki MN. Study of multilevel programming in programmable metallization cell (PMC) memory. IEEE Transactions on Electron Devices. 2009;**56**(5):1040-1047. DOI: 10.1109/TED.2009.2016019

[53] Zhuge F, Li K, Fu B, Zhang H, Li J, Chen H, et al. Mechanism for resistive switching in chalcogenide-based electrochemical metallization memory cells. AIP Advances. 2015;**5**(5):057125. DOI: 10.1063/1.4921089

[54] Tian X, Yang S, Zeng M, Wang L, Wei J, Xu Z, et al. Bipolar electrochemical mechanism for mass transfer in nanoionic resistive memories. Advanced Materials. 2014;**26**(22):3649-3654. DOI: 10.1002/adma.201400127

[55] Valov I, Waser R. Comment on real-time observation on dynamic growth/dissolution of conductive filaments in oxide-electrolyte-based ReRAM. Advanced Materials. 2013;**25**(2):162-164. DOI: 10.1002/adma.201202592

[56] Aratani K, Ohba K, Mizuguchi T, Yasuda S, Shiimoto T, Tsushima T, et al. A novel resistance memory with high scalability and nanosecond switching. In: 2007 IEEE International Electron Devices Meeting (IEDM): Technical Digest; Dec. 10-12, 2007; Washington DC, USA. Piscataway, NJ, USA: IEEE; 2007. pp. 783-786. DOI: 10.1109/IEDM. 2007.4419064

[57] Yoon Y, Choi H, Lee D, Park JB, Lee J, Seong DJ, et al. Excellent switching uniformity of Cu-doped MoO_x/GdO_x bilayer for nonvolatile memory applications. IEEE Electron Device Letters. 2009;**30**(5):457-459. DOI: 10.1109/LED.2009.2015687

[58] Chen YY, Govoreanu B, Goux L, Degraeve R, Fantini A, Kar GS, et al. SET/RESET pulse for $>10^{10}$ endurance in HfO_2/Hf 1T1R bipolar RRAM. IEEE Transactions on Electron Devices. 2012;**59**(12):3243-3249. DOI: 10.1109/TED.2012.2218607

[59] Balatti S, Ambrogio S, Wang ZQ, Sills S, Calderoni A, Ramaswamy N, Ielmini D. Pulsed cycling operation and endurance failure of metal-oxide resistive (RRAM). In: 2014 IEEE International Electron Devices Meeting (IEDM): Technical Digest; Dec. 15-17, 2014; San Francisco, CA, USA. Piscataway, NJ, USA: IEEE; 2014. pp. 14.3.1-14.3.4. DOI: 10.1109/IEDM.2014.7047050

[60] Shenoy RS, Gopalakrishnan K, Jackson B, Virwani K, Burr GW, Rettner CT, et al. Endurance and scaling trends of novel access-devices for multi-layer crosspoint-memory based on mixed-ionic-electronic-conduction (MIEC) materials. In: 2011 Symposium on VLSI Technology: Digest of Technical Papers; June 14-16, 2011; Kyoto, Japan. Piscataway, NJ, USA: IEEE; 2011. pp. 94-95

[61] Kinoshita K, Tsunoda K, Sato Y, Noshiro H, Yagaki S, Aoki M, Sugiyama Y. Reduction in the reset current in a resistive random access memory consisting of NiO_x brought about by reducing a parasitic capacitance. Applied Physics Letters. 2008;**93**(3):033506. DOI: 10.1063/1.2959065

[62] Liu CY, Sung PW. Different resistive switching characteristics of a Cu/SiO_2/Pt structure. Japanese Journal of Applied Physics. 2011;**50**(9R):091101. DOI: 10.1143/JJAP.50.091101

[63] Wei Z, Kanzawa Y, Arita K, Katoh Y, Kawai K, Muraoka S, et al. Highly reliable TaO_x ReRAM and direct evidence of redox reaction mechanism. In: 2008 IEEE International Electron Devices Meeting (IEDM): Technical Digest; Dec. 15-17, 2008; San Francisco, CA, USA. Piscataway, NJ, USA: IEEE; 2008. pp. 1-4. DOI: 10.1109/IEDM.2008.4796676

IntechOpen